DEPARTMENT REPORT UWME-DR-201-101-1

MICROMECHANICAL PREDICTIONS OF CRACK PROPAGATION AND FRACTURE ENERGY IN A SINGLE-FIBER BORON/ALUMINUM MODEL COMPOSITE

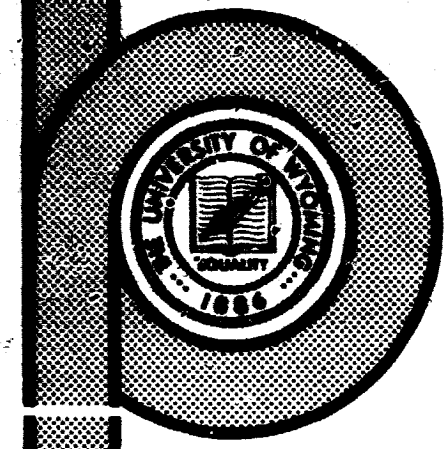

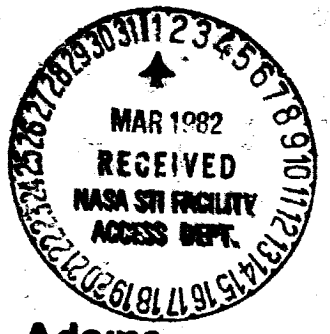

Donald F. Adams
Jayant M. Mahishi

February 1982

TECHNICAL REPORT
NASA-Lewis Research Center
Grant No. NSG-3217

Approved for Public Release: Distribution Unlimited

COMPOSITE MATERIALS RESEARCH GROUP
DEPARTMENT of MECHANICAL ENGINEERING
University of Wyoming **Laramie, Wyoming 82071**

DEPARTMENT REPORT
UWME-DR-201-101-1

MICROMECHANICAL PREDICTIONS OF CRACK PROPAGATION AND FRACTURE ENERGY IN A SINGLE-FIBER BORON ALUMINUM MODEL COMPOSITE

DONALD F. ADAMS
JAYANT M. MAHISHI

FEBRUARY 1982

TECHNICAL REPORT
NASA-LEWIS RESEARCH CENTER
GRANT NO. NSG-3217

COMPOSITE MATERIALS RESEARCH GROUP
MECHANICAL ENGINEERING DEPARTMENT
UNIVERSITY OF WYOMING
LARAMIE, WYOMING 82071

1 Report No	2 Government Accession No	3 Recipient's Catalog No

4 Title and Subtitle	5 Report Date
Micromechanic l Predictions of Crack Propagation and Fracture Energy in a Single-Fiber Boron/Aluminum Model Composite	February 1982
	6 Performing Organization Code
7 Author(s)	8 Performing Organization Repo t No
Donald F. Adams and Jayant M. Mahishi	UWME-DR-201-101-1
	10 Work Unit No
9 Performing Organization Name and Address Composite Materials Research Group University of Wyoming Laramie, WY 82071	11 Contract or Grant No NSG-2317
	13 Type of Report and Period Covered Technical Report
12 Sponsoring Agency Name and Address NASA-Lewis Research Center 21000 Brookpark Road Cleveland, OH 44135	14 Sponsoring Agency Code

15 Supplementary Notes

Program Monitor:
Dr. J. A. DiCarlo
Materials Science Branch

16 Abstract

The axisymmetric finite element model and associated computer program developed for the analysis of crack propagation in a composite consisting of a single broken fiber in an annular sheath of matrix material has been extended to include a constant displacement boundary condition during an increment of crack propagation. The constant displacement condition permits the growth of a stable crack, as opposed to the catastropic failure in an earlier version.

The finite element model has been refined, to respond more accurately to the high stresses and steep stress gradients near the broken fiber end. The accuracy and effectiveness of the conventional constant strain axisymmetric element for crack problems have been established by solving the classical problem of a penny-shaped crack in a thick cylindrical rod under axial tension. The stress intensity factors predicted by the present finite element model are compared with existing continuum results.

Six different failure theories have been incorporated, and used to establish first failure. The crack is also propagated as dictated by the selection of any one of these theories. The ultimate tensile strengths predicted by each of these failure theories have also been compared, and an attempt has been made to quantitatively evaluate actual rate of energy absorption during crack propagation.

17 Key Words (Suggested by Author(s))	18 Distribution Statement
Boron/Aluminum Composites Metal Matrix Composites Micromechanics Analysis Energy Absorption Crack Propagation	Unclassified, Unlimited

19 Security Classif (of this report)	20 Security Classif (of this page)	21 No of Pages	22 Price*
Unclassified	Unclassified	60	

For sale by the National Technical Information Service Springfield Virginia 22161

PREFACE

This annual Technical Report presents research conducted during the third year of NASA-Lewis Grant NSG-3217. The NASA-Lewis Technical Monitor since the inception of this grant has been Dr. J. A. DiCarlo of the Materials Science Branch.

This study is being performed within the Composite Materials Research Group at the University of Wyoming. The Principal Investigator is Dr. Donald F. Adams, Professor of Mechanical Engineering. Mr. J. M. Mahishi, Ph.D. student in Mechanical Engineering, performed the work contained herein, as part of his research assistantship duties within the Composite Materials Research Group.

TABLE OF CONTENTS

SECTION 1

INTRODUCTION

The present report includes work performed during the third year of a NASA-Lewis grant to study the energy absorption mechanisms during crack propagation in metal matrix composites.

The report of the first-year work [1] contains a literature review covering the general area of micromechanics analyses of unidirectional composites, as related to the present study. During the first year, an existing elastoplastic, generalized plane strain, finite element micromechanics analysis [2-4] was modified to include crack propagation, following the general procedure developed earlier by Adams [5-8]. Both longitudinal and transverse cross section models were used to study the influence of a broken fiber on inelastic stress distributions.

During the second-year study reported in Reference [9], the generalized plane strain crack propagation procedure was refined, and detailed results obtained. The analysis was also reformulated for an axisymmetric model. This alternate two-dimensional analysis retained all of the general features of the generalized plane strain version. Its intended primary application was to permit the study of a simple model composite consisting of a single broken fiber in a circular cylindrical sheath of matrix material. The boundary condition selected during a crack propagation increment was constant applied stress. While a realistic condition, it resulted in a crack propagating catastropically once it initiated.

During the present third-year study, this boundary condition has been altered so that a constant boundary displacement can be maintained during

an increment of propagation. Thus, the applied stress reduces as the crack propagates, resulting in crack arrestment. This boundary condition is representative of what can be readily simulated in a laboratory environment, using a testing machine in its displacement-control mode.

Having the ability to simulate the propagation of a stable crack, the present report focuses on the energy dissipation and fracture response of a single broken boron fiber in a sheath of aluminum matrix material, as a composite model which could be readily correlated with experimental data.

SECTION 2

AXISYMMETRIC FINITE ELEMENT MODEL

One purpose of the axisymmetric model as described in Reference [9] was to provide supporting correlations with the two-dimensional, generalized plane strain longitudinal and traverse cross section models. However, an even more important purpose is to provide analytical results for comparison with proposed experiments under similar conditions, i.e., a single broken boron fiber surrounded by a uniform annular sheath of aluminum matrix, as shown in Figure 1. The formulation of the required axisymmetric element and the corresponding computer program are presented in Reference [9]. The finite element and the computer program were fully developed and some preliminary results were presented. However, it was noted that the initiation of a crack in the single fiber axisymmetric model led almost immediately to a catastropic failure of the composite. Thus, the results were not useful from an experimental correlation point of view, which requires the determination of measurable quantities such as crack opening displacements and surface strains during the process of crack extension. For experimental verification purposes, a constant boundary displacement crack propagation scheme has been implemented in the program during the present study, which ensures stable crack propagation.

It was also felt that the number of elements used in the previous study [9] was inadequate to represent the high stress gradients which occur near broken fiber ends. A refined model was evolved, shown in Figure 2, having 840 elements, nearly 400 of which are concentrated near the broken fiber end. An automated triangular element mesh generation routine [10] has been implemented for more accurate and efficient grid data generation.

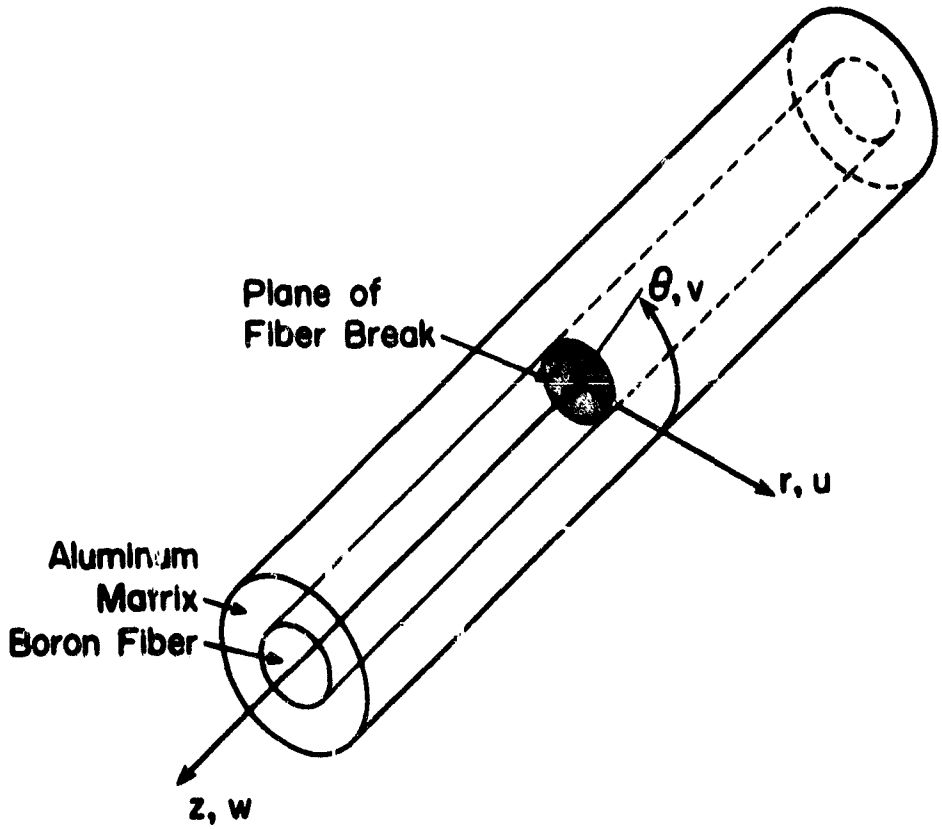

Figure 1. Axisymmetric Analysis Model of a Single Broken Fiber in a Sheath of Matrix Material

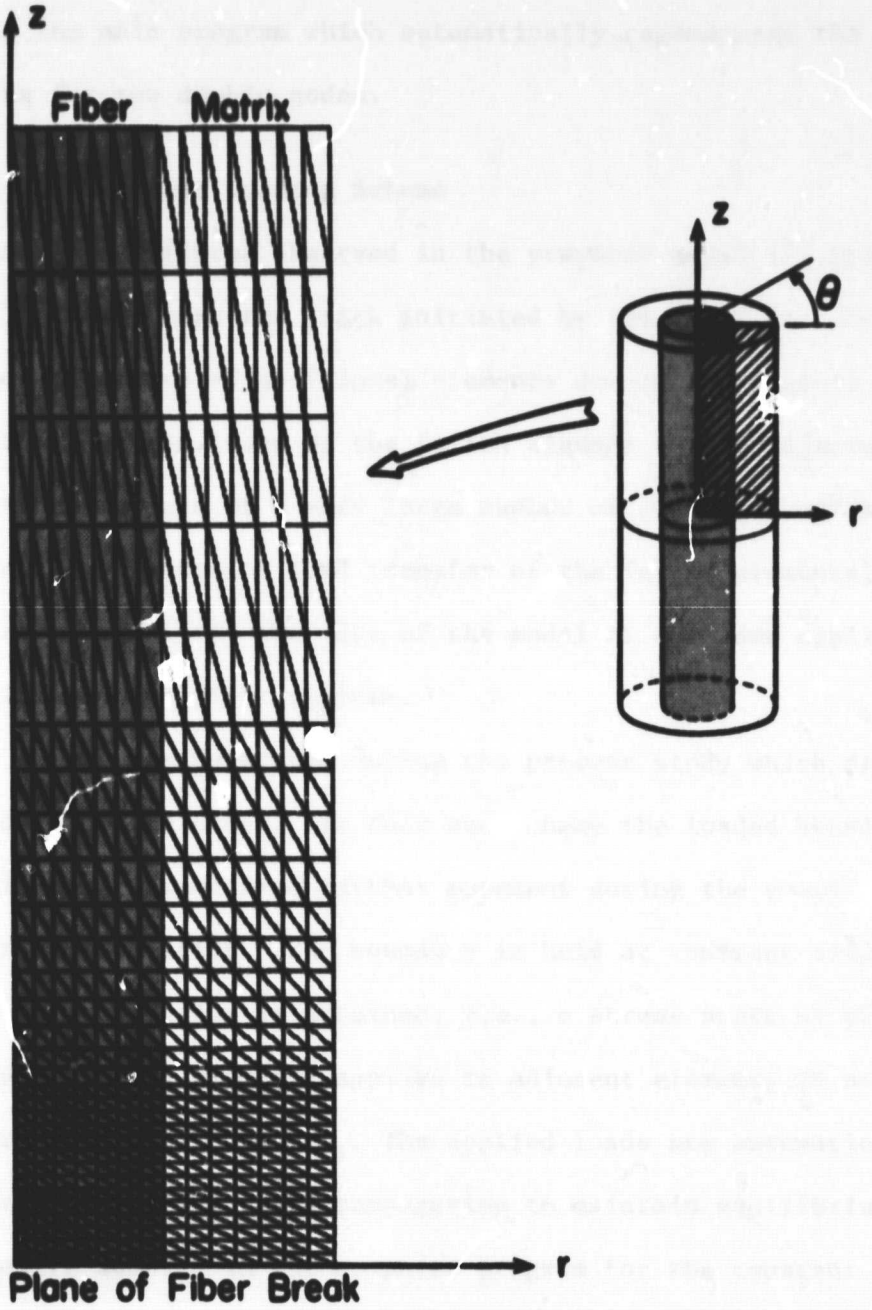

Figure 2. Finite Element Grid Utilized

A special double node concept has been used at the junction of the broken fiber end and the surrounding matrix, as shown in Figure 3, to more accurately represent actual physical conditions. A routine has been implemented in the main program which automatically regenerates the mesh data accounting for the double nodes.

2.1 Constant Displacement Loading Scheme

The catastropic failures observed in the previous model [9] were attributed to the fact that the crack initiated by the first failure of an element led to failure of additional elements during the process of transferring the reaction loads of the failed element to the adjacent elements. Further failure of a very large number of elements was observed during the process of reaction load transfer of the failed elements, growing the crack rapidly to the edge of the model at the same applied load which initiated the first failure.

A simple scheme was developed during the present study which prevents such rapid growth of the crack. In this new scheme the loaded boundary of the specimen is constrained from further movement during the ensuing crack propagation after initiation. The boundary is held at constant displacement until a state of equilibrium is attained, i.e., a stress state at which the reaction loads of failed elements applied to adjacent elements do not lead to any further failure of elements. The applied loads are automatically continuously reduced during crack propagation to maintain equilibrium.

The procedure adopted in the computer program for the constant displacement condition is as follows. After assembling the stiffnesses of each of the individual elements into a banded global stiffness matrix of the form [2]

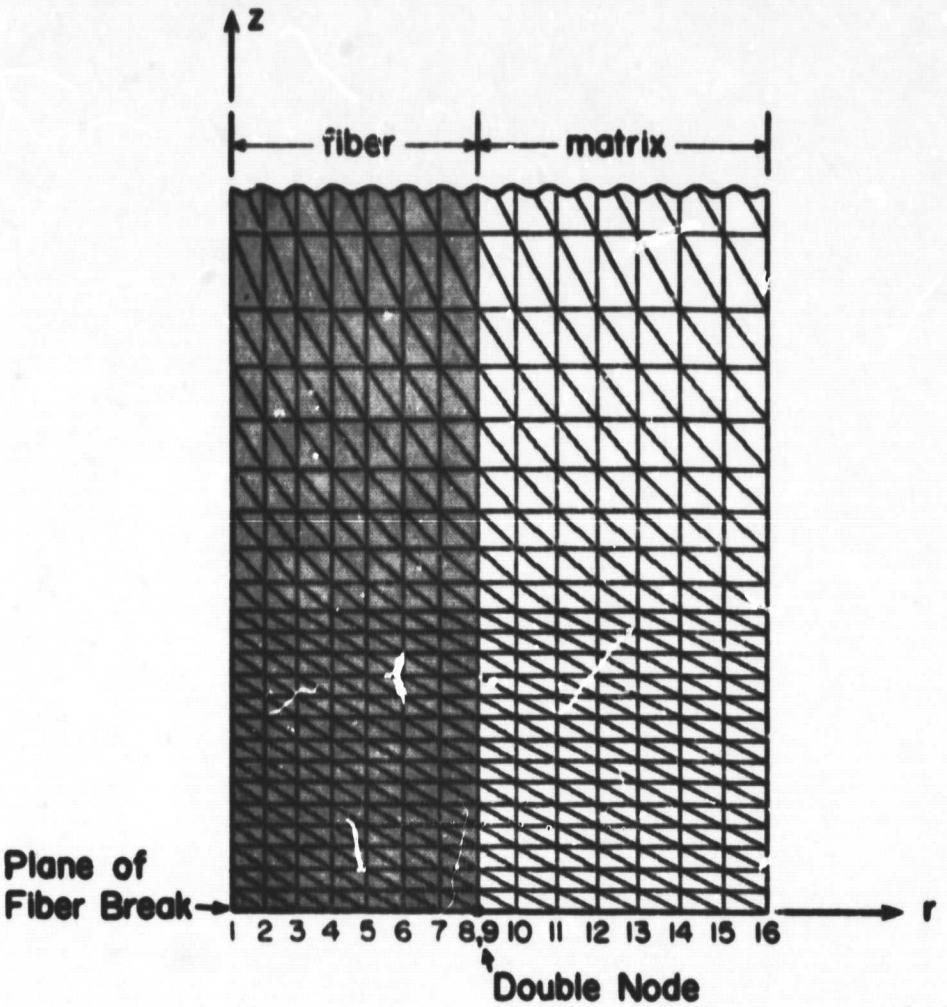

Figure 3. Double Node System Used at the Broken Fiber End

$$\begin{Bmatrix} F_1 \\ F_2 \\ \cdot \\ \cdot \\ \cdot \\ F_n \end{Bmatrix} = \begin{bmatrix} K_{11} & K_{12} \cdots K_{1n} \\ K_{22} & K_{23} \\ \cdot & \\ \cdot & \\ \cdot & \\ K_{nn} \end{bmatrix} \begin{Bmatrix} u_1 \\ u_2 \\ \cdot \\ \cdot \\ \cdot \\ u_n \end{Bmatrix} \tag{1}$$

where {F} is the load vector, {u} is the displacement vector, and [K] is the global stiffness matrix.

The maintenance of a condition of uniform axial displacement of both fiber and matrix at the loading boundary necessitates the use of the Branca boundary condition technique [11]. This technique as adapted to the micromechanics analysis has been explained in detail in References [1, 2, 9]. In this technique, the equations representing the axial displacements of all loaded boundary nodes are added to the equation corresponding to the axial displacement at the corner of the region of interest (i.e., to the axial displacement equation representing the extreme right loading edge boundary node, which is numbered last for convenience in identifying it).

The constant boundary displacement condition is easily applied by setting the value of the stiffness in the last equation, which corresponds to the displacement of the entire loading boundary, to a very large number after the initiation of the crack. A value of 10^{30} psi has been used in the present analysis.

The value of the load reduction which results when the displacement is constrained is obtained by multiplying the displacement vector with the stiffness coefficients corresponding to the last boundary node axial displacement, i.e.,

$$\{\bar{F}_z\} = [\bar{K}]\{u\} \tag{2}$$

2.2 Boundary Conditions

The constant lateral displacement boundary conditions applied in the original version of the axisymmetric model [9] have been removed as they do not adequately represent physical conditions. The outer surface of the matrix is now free to deform in any direction.

During the present analysis, it was found that the common node point for both fiber and matrix at the outer radius of the broken fiber, on the plane of the fiber break, led to very high stress concentrations in the fiber material. The reason for the presence of these large stress concentrations was found to be due to the modeled continuity of the supposedly completely broken fiber at the common node. In order to represent the actual conditions of total discontinuity of the fiber at the break while retaining the continuity of the matrix material at the same point, a double node approach has been incorporated. Two separate node numbers are assigned at the same point (Figure 2), one being considered to be associated with the fiber material and the other with the matrix material. The boundary conditions are applied such that the node point in the fiber is allowed to have both axial and radial displacements (i.e., it is free to move in both the axial and radial directions) while the node point in the matrix is constrained by the symmetry conditions to have only a radial displacement. Actually, both of these nodes (Nodes 8 and 9 in Figure 2) should also be constrained to have the same radial displacement. However, this would lead to the task of implementing a constrained equation capability in the program. By experimenting with the program it was found that the affect of the absence of this constrained displacement condition on the results was not significant and could be neglected. In practice, the element in the matrix at the broken fiber end typically fails early in the loading process, making this node ineffective as the element itself will not be effective any longer.

2.3 Failure Criteria

The failure of interest in the present study is that of the matrix material, which is exhibited as a matrix crack initiation at the tip of the pre-existing crack or fiber break. This crack then propagates with increasing applied load, corresponding to successive failures of finite elements in the vicinity of the crack t

The matrix is typically an isotropic material (although the analysis is not restricted to this assumption). There are a considerable number of failure criteria available, many of which have been used in connection with composite material analyses.

In the prior version of the present axisymmetric model analysis [1, 9], an octahedral shear stress failure criterion was used. In the present study, it was found that this failure criterion did not always lead to realistic results. Thus, the analysis and related computer program was modified to permit the selection of any one of six different failure criteria, at the user's option. These six criteria are presented in Table 1. Example results and additional discussion will be presented later, in Section 5 of this report.

The use of the axisymmetric model, with all of these modifications incorporated, is demonstrated by a series of numerical examples in the following sections. In the next section, Section 3, the properties of the boron fiber and aluminum matrix utilized are presented. These are the same as those used in the two prior reports [1,9]. Thus, direct comparisons can be made for all results presented here.

The axisymmetric finite element model is first applied to a solid aluminum rod containing a central penny-shaped crack, in Section 4.1. The results are compared with those obtained using other (closed form) methods, thus establishing the performance of the finite element model. Then, in Section 4.2,

Table 1

Failure Theory Options Available in the Present Analysis

Failure Theory	Mathematical Form	References
Maximum Normal Stress	Fracture is assumed tc have occurred if any one of the following inequalities is satisfied:* $\sigma_1 \geq X_t, Y_t$ $\sigma_1 \leq X_c, Y_c$ $\sigma_2 \geq X_t, Y_t$ $\sigma_2 \leq X_c, Y_c$ $\sigma_\theta \geq X_t, Y_t$ $\sigma_\theta \leq X_c, Y_c$ where σ_1, σ_2 and σ_θ are principal stresses, and subscripts t and c indicate tension and compression, respectively	12, 13, 14, 16
Maximum Shear Stress	$\tau_{12} \geq S$ where τ_{12} = maximum shear stress = $\frac{\sigma_1 - \sigma_2}{2}$	12, 13, 14, 16
Octahedral Shear Stress	$\tau_{oct} \geq \tau_{o_{ult}}^{**}$ where τ_{oct} = octahedral shear stress $= 1/3\sqrt{(\sigma_r-\sigma_z)^2+(\sigma_z-\sigma_\theta)^2+(\sigma_\theta-\sigma_r)^2+6\tau_{rz}^2}$	13, 14, 16
Tsai-Hill	$\frac{\sigma_z^2}{X_t^2} + \frac{\sigma_r^2}{Y_t^2} + \frac{\sigma_\theta^2}{Y_t^2} - \frac{\sigma_r\sigma_z}{X_t^2} - \frac{\sigma_z\sigma_\theta}{X_t^2} - \frac{\sigma_r\sigma_\theta}{Y_t^2} + \frac{\tau_{rz}^2}{S^2} \geq 1$	14, 15, 15, 17, 20
Hoffman	$\left(\frac{1}{X_t} + \frac{1}{X_c}\right)\sigma_z + \left(\frac{1}{Y_t} + \frac{1}{Y_c}\right)\sigma_r + \frac{\sigma_z^2}{X_tX_c} + \frac{\sigma_r^2}{Y_tY_c} - \frac{\sigma_z\sigma_r}{X_tX_c} + \frac{\tau_{rz}^2}{S^2} \geq 1$	14, 15, 16, 17, 20
Tsai-Wu (Modified)	$\left(\frac{1}{X_t} + \frac{1}{X_c}\right)\sigma_z + \left(\frac{1}{Y_t} + \frac{1}{Y_c}\right)\sigma_r - \frac{\sigma_z^2}{X_tX_c} - \frac{\sigma_r^2}{Y_tY_c} + \frac{\tau_{rz}^2}{S^2} \geq 1$	12, 15, 18, 19, 20

* X, Y, S are ultimate axial, transverse and shear strengths, respectively

** Ultimate octahderal shear stress ($\sqrt{2}/3\ X_t$)

detailed results are presented for various boron/aluminum composite models. Finally, in Section 4.3, energy absorption associated with crack propagation is discussed.

SECTION 3

MATERIAL PROPERTIES

In modeling the boron/aluminum composite, the boron fibers have been treated as brittle, linearly elastic materials with isotropic strength and stiffness properties. The aluminum matrix has also been considered to be isotropic, but is modeled as an elastoplastic material. To accomplish this, the actual stress-strain curve of the aluminum alloy selected is input to the analysis by curve fitting via a Richard-Blacklock two-parameter equation [21], as discussed in Appendix A-5 of Reference [1]. Thus, at any load level the tangent modulus for any given element can be computed. This makes possible an accurate representation of the plastic deformation of the matrix.

Although the nonlinear material properties of any matrix material, e.g., another aluminum alloy, can readily be incorporated in the analysis, a 6061-T6 aluminum alloy at 75°F was used in obtaining the present results. The material properties shown in Table 1 were obtained from Reference [22]; the full range stress-strain curve for determining the curve-fit parameters used is shown in Figure 4.

Table 2

6061-T6 Aluminum Alloy Matrix Material Properties [22]

Young's Modulus	$E = 10.0 \times 10^6$ psi
Poisson's Ratio	$\nu = 0.33$
Tensile Yield Strength	$F^{ty} = 36000$ psi
Tensile Ultimate Strength	$F^{tu} = 45000$ psi
Coefficient of Thermal Expansion	$\alpha = 13.0 \times 10^{-6}/°F$

The boron fiber properties indicated in Table 3 were obtained from Reference [23].

Table 3

Boron Fiber Material Properties [23]

Young's Modulus	$E = 60.5 \times 10^6$ psi
Poisson's Ratio	$\nu = 0.13$
Tensile Ultimate Strength	$F_{tu} = F_{ty} = 500{,}000$ psi
Ultimate Strain	$\varepsilon_{tu} = \frac{F_{tu}}{E} = 8.264 \times 10^{-3}$ in./in.
Coefficient of Thermal Expansion	$\alpha = 9.0 \times 10^{-6}$/°F

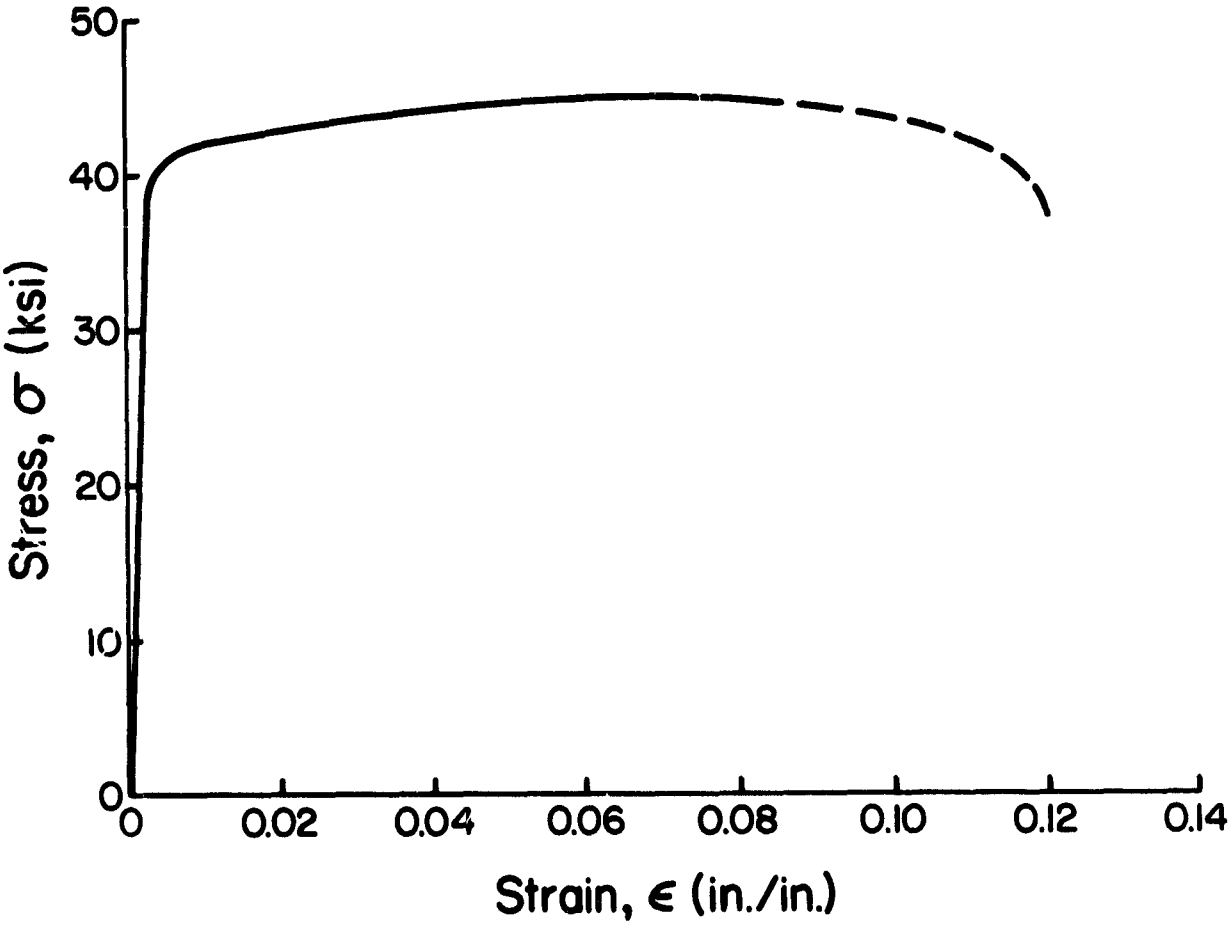

Figure 4. Typical Full Range Stress-Strain Curve for 6061-T6 Aluminum Alloy at Room Temperature [22].

SECTION 4

NUMERICAL RESULTS

4.1 Evaluation of the Axisymmetric Finite Element Model for Crack Problems in General

According to linear elastic fracture mechanics (LEFM) theories, a crack will begin to propagate when the amplitude of the stress field in the immediate vicinity of the crack tip (the stress intensity factor) reaches a critical value. Thus, the prediction of stress intensity factors for different geometric conditions assumes major importance in LEFM theories.

Even though the present finite element model and related computer program are not limited by linear elasticity assumptions, it was decided to first evaluate the performance of the model under this most severe case of singular stresses near the crack tip.

4.1.1 Application of Conventional Elements

A considerable amount of work has been done in the area of finite element applications to LEFM problems, and a number of two-dimensional and three-dimensional elements with embedded singularities are now available. However, conventional elements, even though they do not adequately represent the singular state of stress, can be used for rather accurate estimations of stress intensity factors by proper interpretation of the results.

There are two different techniques for calculating stress intensity factors from conventional element solutions. The first technique requires a very fine grid near the crack tip to obtain a very accurate description of the displacement field. These displacements are then substituted into the classical continuum solution to obtain the stress intensity factors. In the second technique, the strain energy of the system with a crack is

calculated for two slightly different crack lengths. The strain energy release rate during the crack extension gives the stress intensity factors directly.

4.1.2 Axisymmetric Crack Problems

The two types of axisymmetric cracks in an axisymmetric body that can be analyzed using the axisymmetric finite element method are a central penny-shaped crack and a circumferential crack. In the present verification example, only a central penny-shaped crack in an aluminum rod subjected to axial tension will be utilized.

The basic equations of linear fracture mechanics are [11,24]

$$\sigma_r = \frac{K_I}{(2\rho)^{\frac{1}{2}}} \cos(\phi/2)[1 - \sin(\phi/2)\sin(3\phi/2)]$$

$$\sigma_z = \frac{K_I}{(2\rho)^{\frac{1}{2}}} \cos(\phi/2)[1 + \sin(\phi/2)\sin(3\phi/2)]$$

$$\tau_{rz} = \frac{K_I}{(2\rho)^{\frac{1}{2}}} \sin(\phi/2)\cos(\phi/2)\cos(3\phi/2) \qquad (3)$$

$$u_r = \frac{K_I(2\rho)^{\frac{1}{2}}}{8G}[(5 - 8\nu)\cos(\phi/2) - \cos(3\phi/2)] + \frac{\alpha\rho}{2G}(1-\nu)\cos\phi + \ldots$$

$$u_z = \frac{K_I(2\rho)^{\frac{1}{2}}}{8G}[(7-8\nu)\sin(\phi/2) - \sin(3\phi/2)] - \frac{\alpha\rho\nu}{2G}\sin\phi + \ldots$$

where

K_I = stress intensity factor

ρ, ϕ = polar coordinates, as shown in Figure 5

G = shear modulus, ν = Poisson's ratio

α = coefficient of second term in the asymptotic expansion [25]

σ_{rr}, σ_{zz}, τ_{rz} = radial, axial and shear stresses

u_r, u_z = radial and axial displacement components

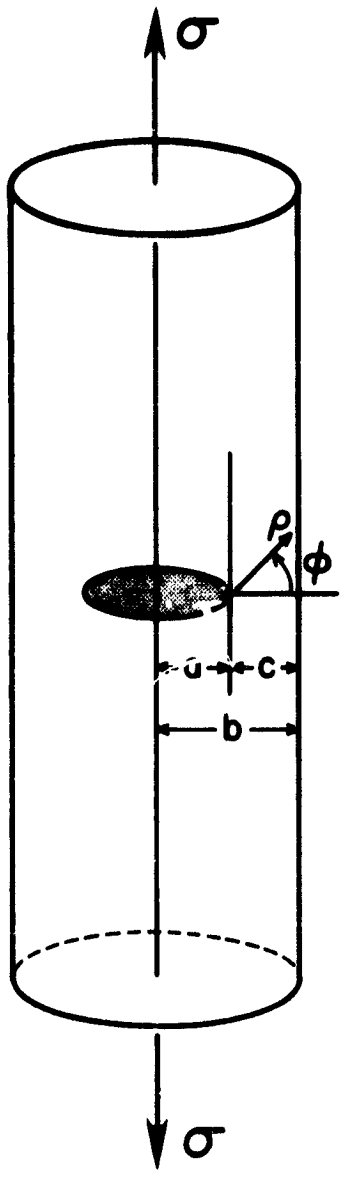

Figure 5. Coordinate System used in Equation (3) and Description of Geometric Parameters used in Equation (4)

The stress intensity factor K_I is calculated from the expressions for u_r and u_z by substituting corresponding values of u_r and u_z obtained from the finite element solution.

For the above case of a central penny-shaped crack in an isotropic thick cylinder subjected to Mode I type loading, there is also a closed form solution available for stress intensity factor, as follows [26-28]:

$$K_I = \frac{\sigma\sqrt{\pi a}}{1-(a/b)^2}\sqrt{\frac{c}{b}}\left[\frac{2}{\pi}\left(1 + \frac{a}{2b} - \frac{5a^2}{8b^2}\right) + 0.268\,\frac{c^3}{b^3}\right] \qquad (4)$$

where a, b and c are geometric parameters, as shown in Figure 5.

4.1.3 Stress Intensity Factors

Penny-shaped cracks of three different radii were analyzed. The overall finite element grid geometry was maintained; the radius of the crack was varied by changing only the boundary conditions. No effort was made to concentrate more elements near the crack tip as the purpose of this linear elastic fracture mechanics example was not so much to accurately determine the stress intensity factor, but rather to evaluate the finite element model to be subsequently used for studying composite behavior. Even better estimates of stress intensity factors would have been possible if that had been the primary purpose.

The estimated stress intensity factors calculated using the present finite element model, and the corresponding values obtained using the closed form solution of Eq. (4), are presented in Table 4.

Table 4

Stress Intensity Factors

r_a/r_b (see Fig. 5)	K_I/σ	
	present finite element analysis	closed form solution (Eq. 4)
0.25	0.531	0.819
0.46	0.809	1.112
0.84	1.647	1.698

Since the stress intensity factors are calculated using the displacement components obtained from the finite element solution, they are very sensitive to the accuracy of the displacement field. Since the constant strain triangular element only allows linear variations of displacements within each element, a better representation of the displacement field can be achieved by having a larger number of smaller elements near the crack tip.

4.1.4 Inelastic Crack Propagation in an Aluminum Bar

Having verified the accuracy of the axisymmetric finite element analysis and related computer program in predicting the high localized stress concentrations at the crack tip of a homogeneous, linearly elastic material, as presented in Section 4.1.3, the capability of the analysis to model inelastic material response and crack propagation was exercised. All of the modifications described in Section 2 were incorporated.

The example of the penny-shaped crack in an aluminum bar of circular cross section, used in Sections 4.1.1 through 4.1.3, was extended by increasing the applied axial stress to cause inelastic material response and then crack propagation to failure. The stress-strain response predicted is presented in Figure 6. It should be noted that the stress plotted is the axial stress applied at a large distance from the crack site, i.e., the total

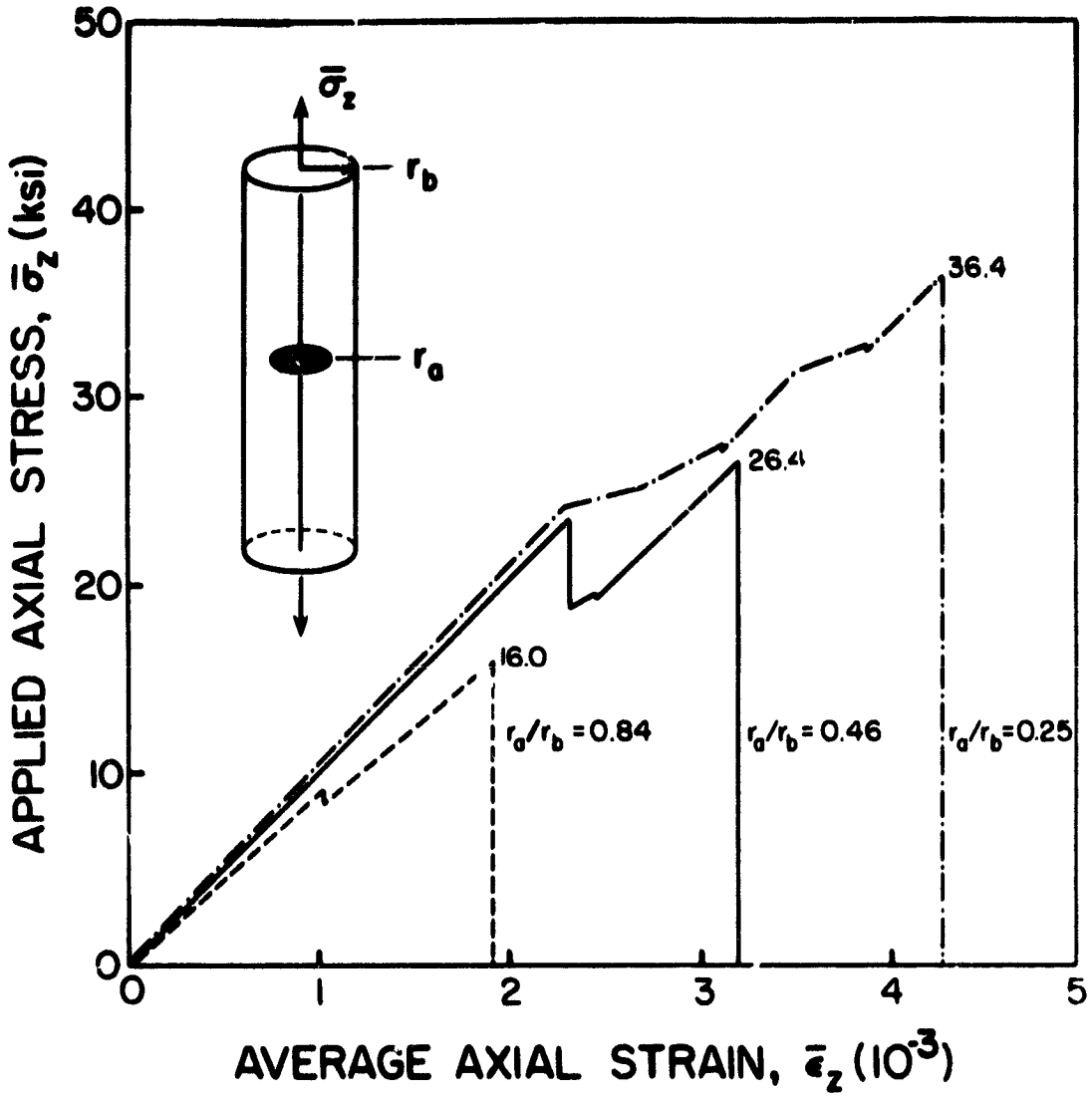

Figure 6. Stress-Strain Response of an Aluminum Circular Rod with Central Penny-Shaped Crack

applied load divided by the gross cross-sectional area. The first abrupt drop in applied axial stress corresponds to the initiation of crack growth, which becomes arrested as the applied stress drops during the constant boundary displacement crack growth increment. The applied stress is then subsequently increased as additional axial loading increments are applied, leading to additional increments of crack growth, until the crack propagates completely outward across the entire cross section.

4.2 Crack Propagation in a Boron/Aluminum Model Composite

The constituent material properties presented in Section 3 were utilized. The single broken fiber model is shown in Figure 1, and the finite element grid utilized is presented in Figures 2 and 3.

The variable studied was the thickness of the aluminum sheath surrounding the broken boron fiber. This has been defined, as in the previous report [9], as the ratio of the radius of the fiber to the radius of the matrix sheath, i.e., r_f/r_m. Three arbitrary radius ratios were analyzed, viz, $r_f/r_m = 0.25$, 0.46, and 0.84, which correspond to fiber volume contents of 6.25, 21.2, and 70.6 percent, respectively.

As in the prior work, no attempt was made to model thermal stress effects due to fabrication processes, although the analysis has this capability. The maximum normal stress failure criterion was used as governing the crack propagation process (see Table 1).

Results are presented in Figure 7. As can be seen, there is a considerable amount of stable crack propagation, as indicated by the many abrupt drops in the applied axial stress. This increased with increasing thickness of the aluminum matrix sheath, as would be expected. Since the area under the stress-strain curve is proportional to the energy absorption capacity of the composite, this stable crack growth is obviously beneficial.

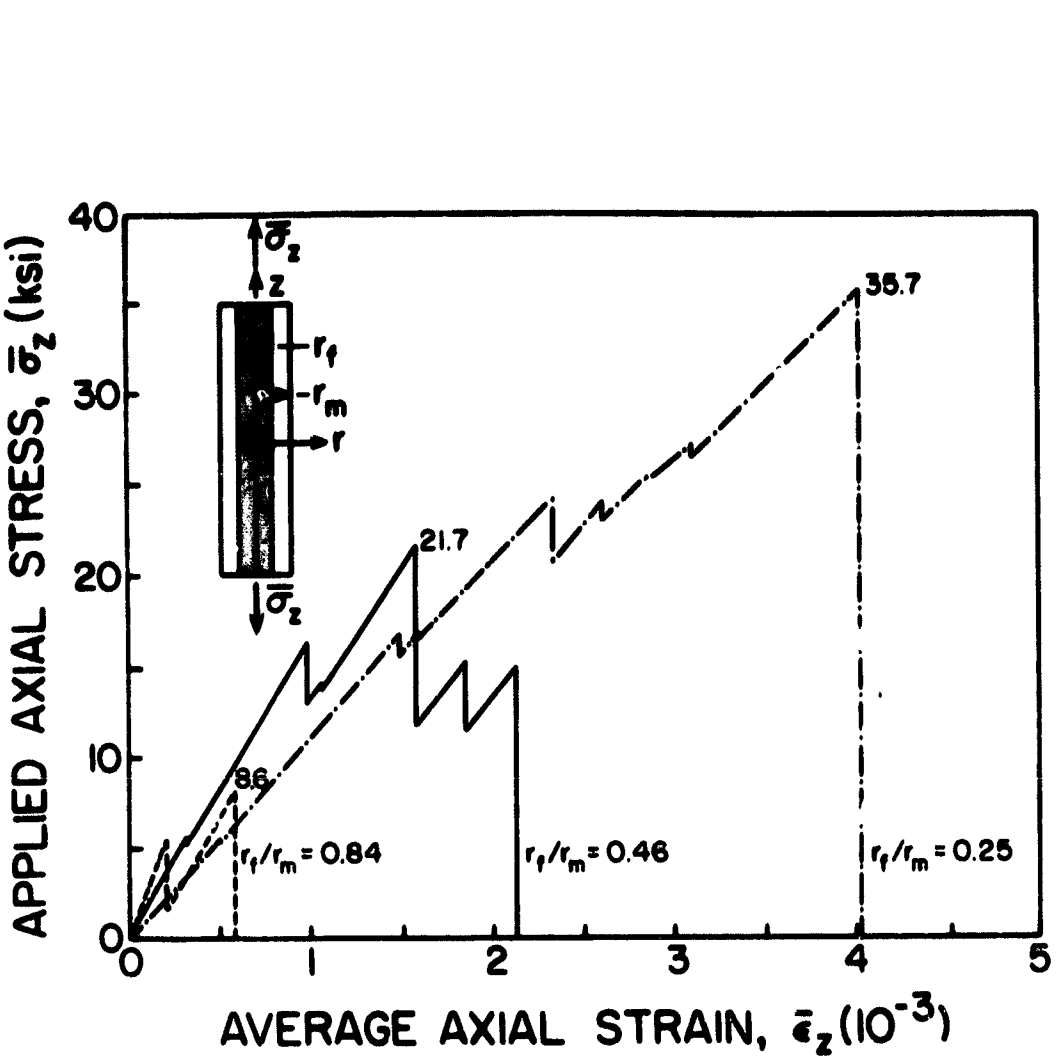

Figure 7. Stress-Strain Response of a Boron/Aluminum Composite with Broken Fiber Under an Axial Applied Stress

Pictorial representations of the crack propagation patterns for each of the r_f/r_m ratios of Figure 7 are shown in Figure 8. The failed elements are shown shaded. The two values of applied axial stress (in units of psi) given under each diagram indicate the stress level (from Figure 7) at which that increment of crack propagation initiated, and arrested. As can be seen, the cracks tended to grow radially outward, with a slight tendency to also grow along the fiber-matrix interface.

The predicted ultimate axial strength for each of the r_f/r_m ratios can also be obtained from Figure 7. These three values are plotted in Figure 9. The value for $r_f/r_m = 0$ represents the ultimate strength of the aluminum matrix (Figure 4 and Table 2), viz, 45 ksi. The value for $r_f/r_m = 1.0$ of zero corresponds to the trivial case of a broken fiber and no aluminum matrix.

While a linear relation between ultimate strength and r_f/r_m is not necessary for this nonlinear material response example, the data of Figure 9 do indicate a relatively linear relation.

An important, longer term objective of the present study is to provide numerical results which can be used to correlate with experimental work as it becomes available. Crack opening displacement would be one such experimental measurement (using X-ray or some similar technique for the present case of the optically opaque aluminum matrix). Figure 10 is a plot of crack opening displacement (defined here as the distance between the two ends of the fiber at the break), for all three r_f/r_m ratios. As can be seen, the predicted displacement values are large enough (in thousandths of an inch) to be readily measured experimentally.

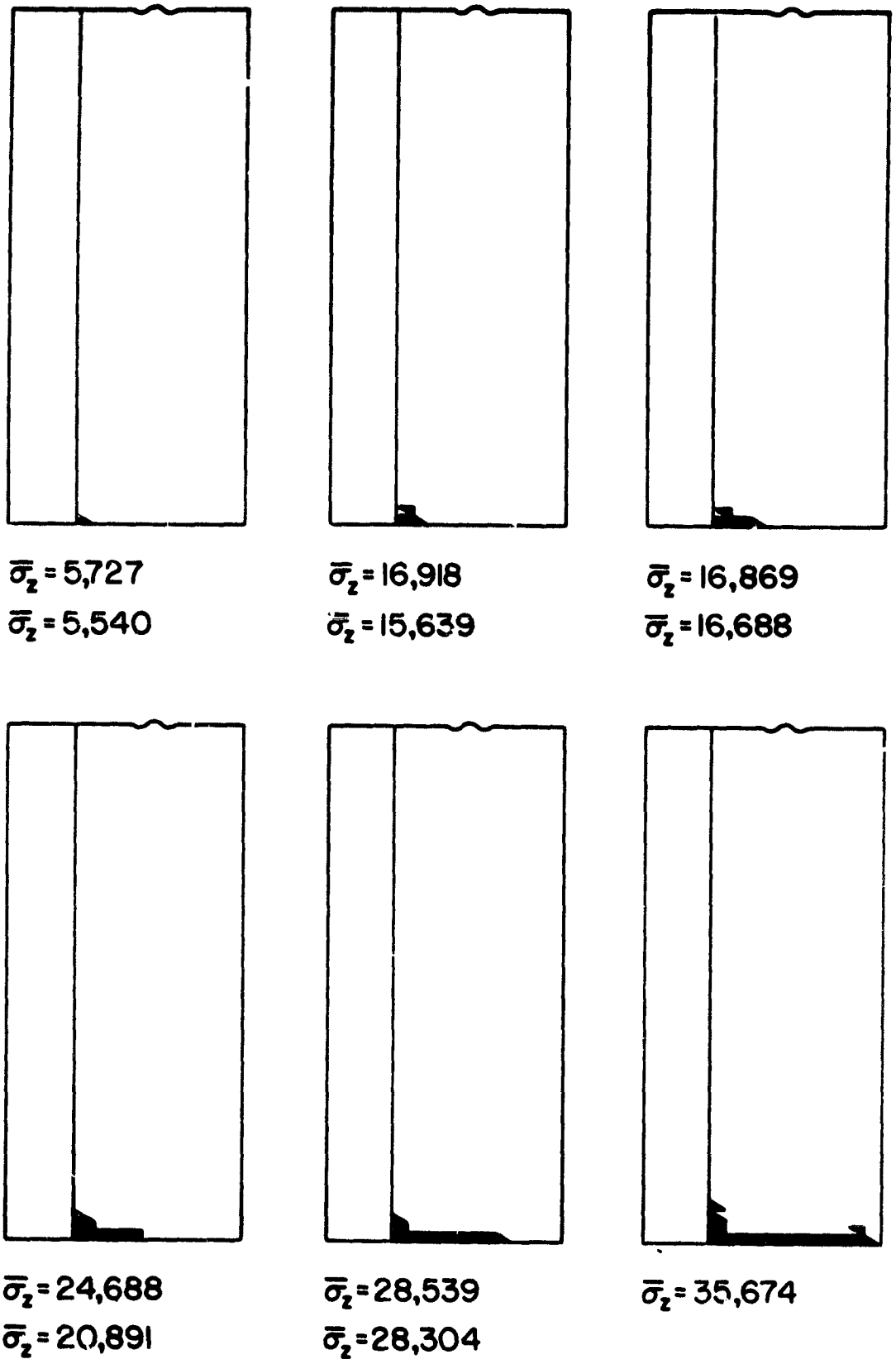

a) r_f/r_m = 0.25

Figure 8. Crack Propagation in a Boron/Aluminum Composite Model as Predicted By the Maximum Normal Stress Theory (stresses in psi)

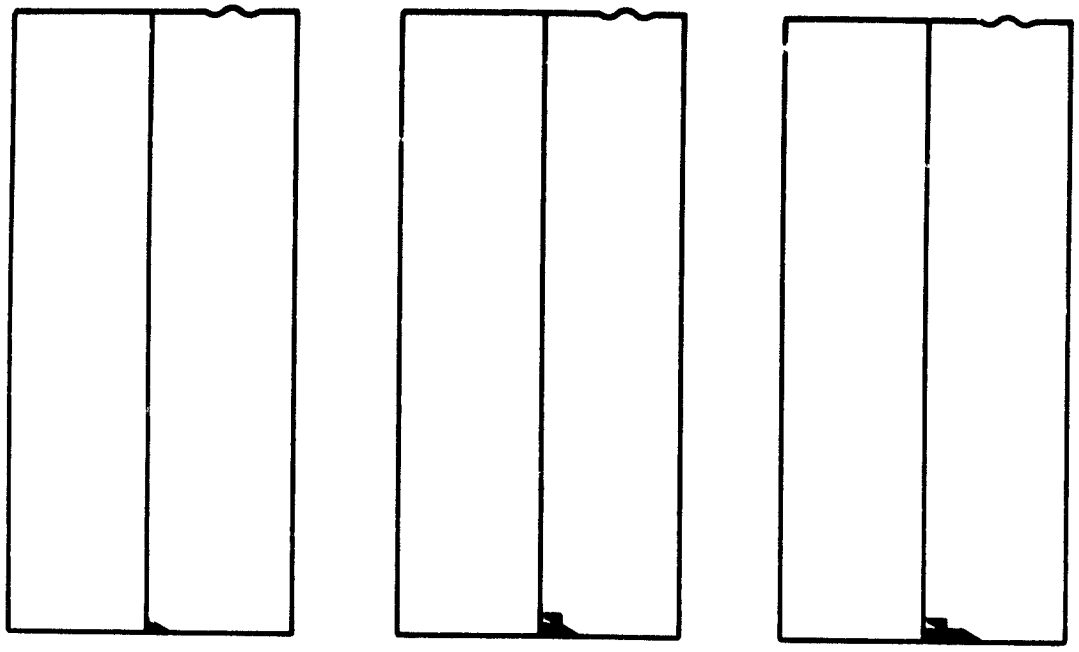

$\bar{\sigma}_z = 5{,}666$
$\bar{\sigma}_z = 5{,}143$

$\bar{\sigma}_z = 16{,}415$
$\bar{\sigma}_z = 12{,}989$

$\bar{\sigma}_z = 14{,}079$
$\bar{\sigma}_z = 13{,}696$

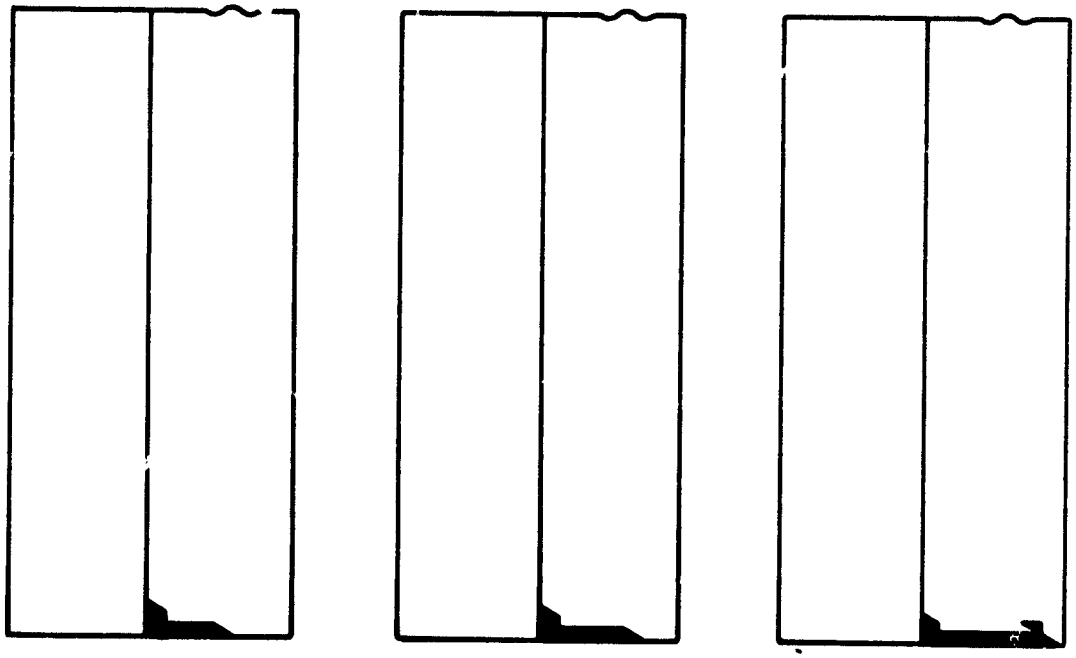

$\bar{\sigma}_z = 21{,}696$
$\bar{\sigma}_z = 11{,}714$

$\bar{\sigma}_z = 15{,}263$
$\bar{\sigma}_z = 11{,}703$

$\bar{\sigma}_z = 15{,}303$

b) $r_f/r_m = 0.46$

Figure 8 (continued)

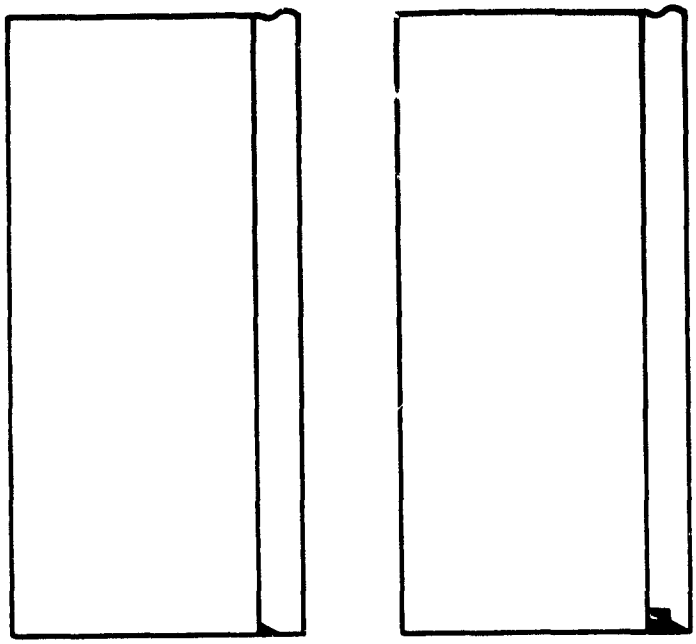

c) $r_f/r_m = 0.84$

Figure 8 (continued)

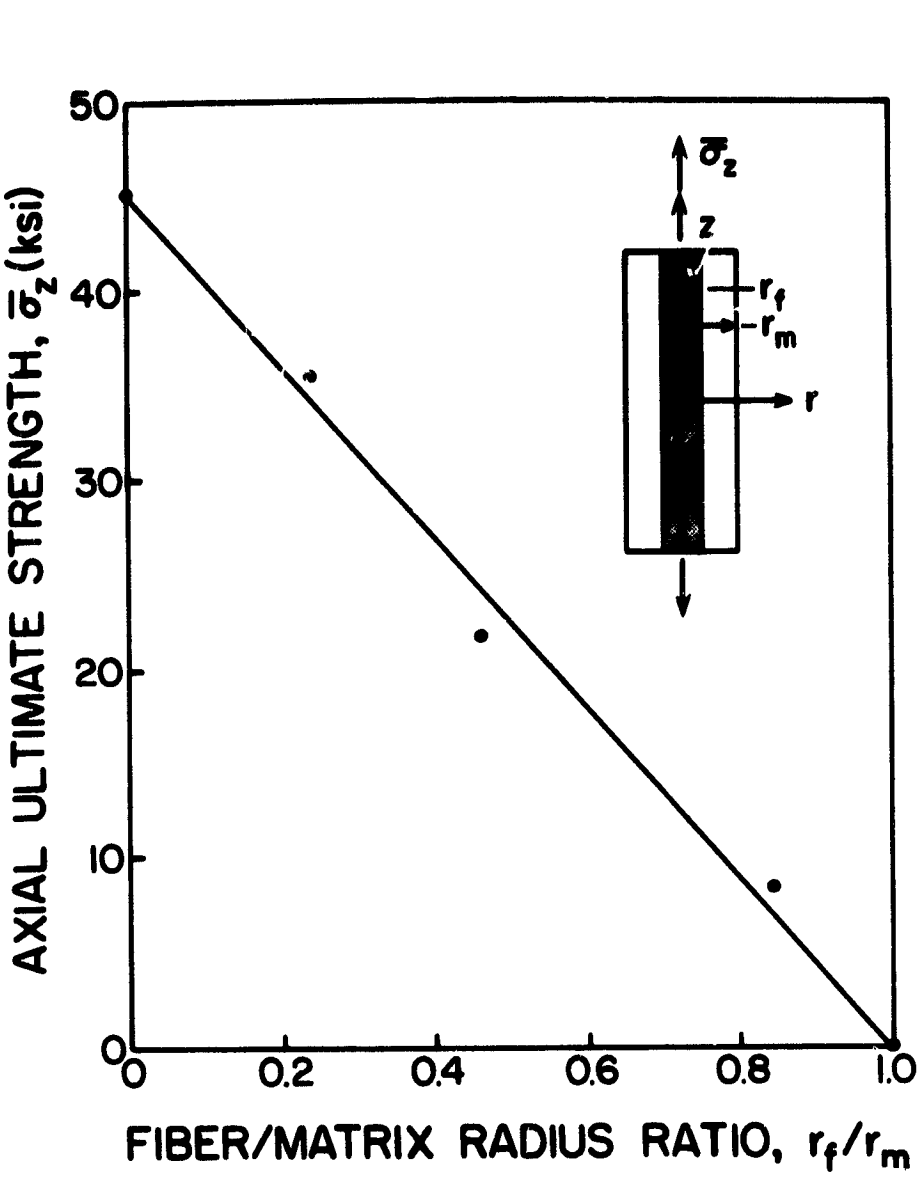

Figure 9. Axial Ultimate Strength Versus Fiber/Matrix Radius Ratio

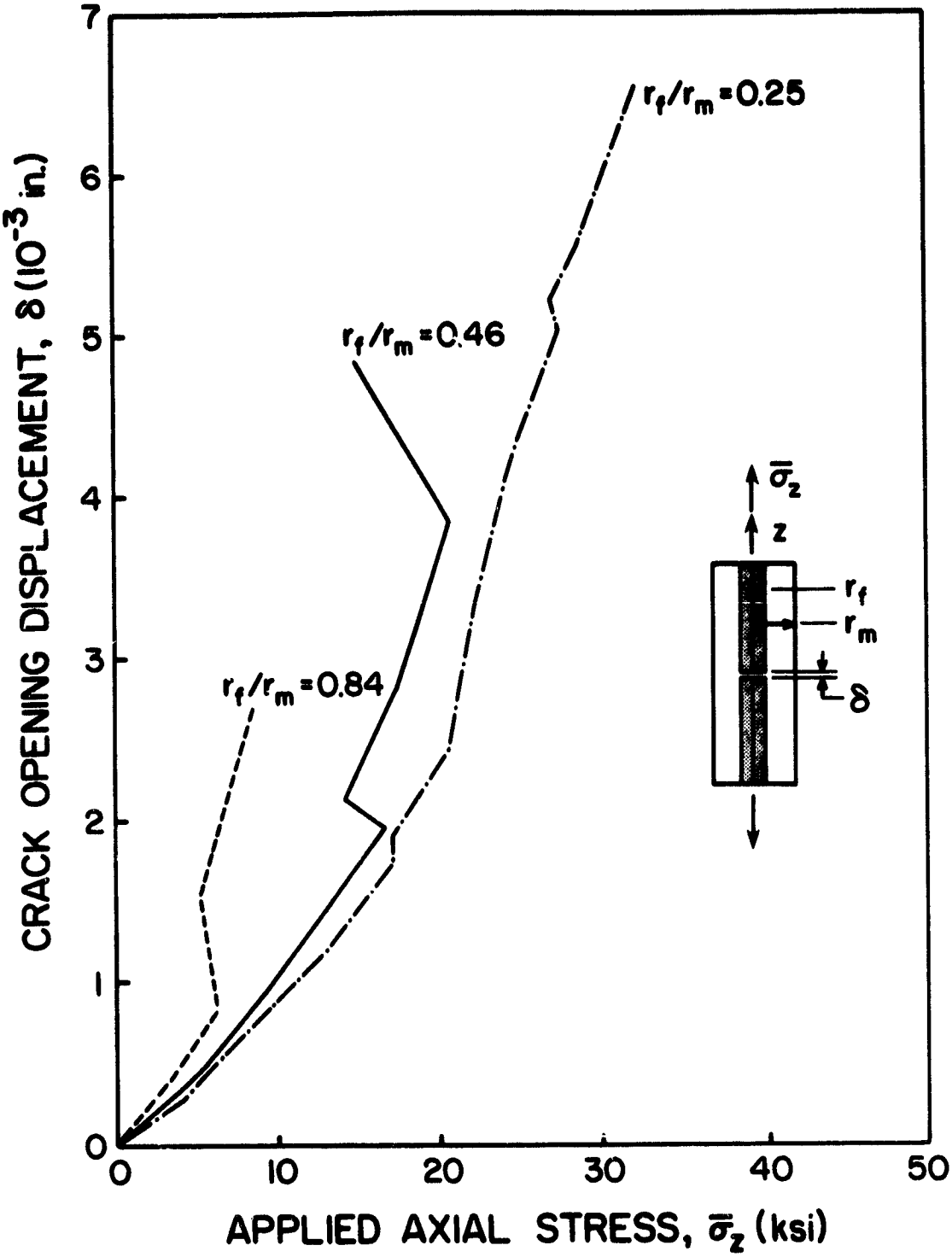

Figure 10. Crack Opening Displacement Versus Applied Axial Stress

It would be simpler, of course, to measure the surface displacement (strain) of the broken-fiber model at the plane of the fiber break. This measurement could be made directly, by using a strain gage or extensometer. Predicted axial strains, ε_z, on the surface of the aluminum matrix at the plane of the fiber break, are plotted in Figure 11 for all three r_f/r_m ratios. The corresponding circumferential strains, ε_θ, are presented in Figure 12. The straight lines corresponding to the strain response of a solid aluminum rod are also given, for comparison purposes.

As can be seen in Figures 11 and 12, the measurement of surface strains is not a very sensitive method of determining the extent of crack propagation.

A practical consideration in attempting correlations with experimental data is how long the numerical model must be to avoid influences of end effects. It is usually desireable to minimize the length of the model, in order to reduce the number of finite elements required, and thus to reduce computing time. The length of the model required can be determined by selecting a length, and then observing how rapidly the stresses return to their undisturbed values away from the discontinuity (the fiber break in the present case). The models used in the present examples were all 4.1 composite model diameters long.

In the case of a single broken fiber in a matrix sheath, the normal stress in the axial direction on a transverse cross section of the fiber remote from the discontinuity will be uniform, as will the normal stress in the matrix sheath. The shear stress will be zero, including the shear stress at the fiber-matrix interface.

Figure 13 is a plot of the axial normal stress distribution across both the fiber and matrix, for the case $r_f/r_m = 0.46$, on cross sections

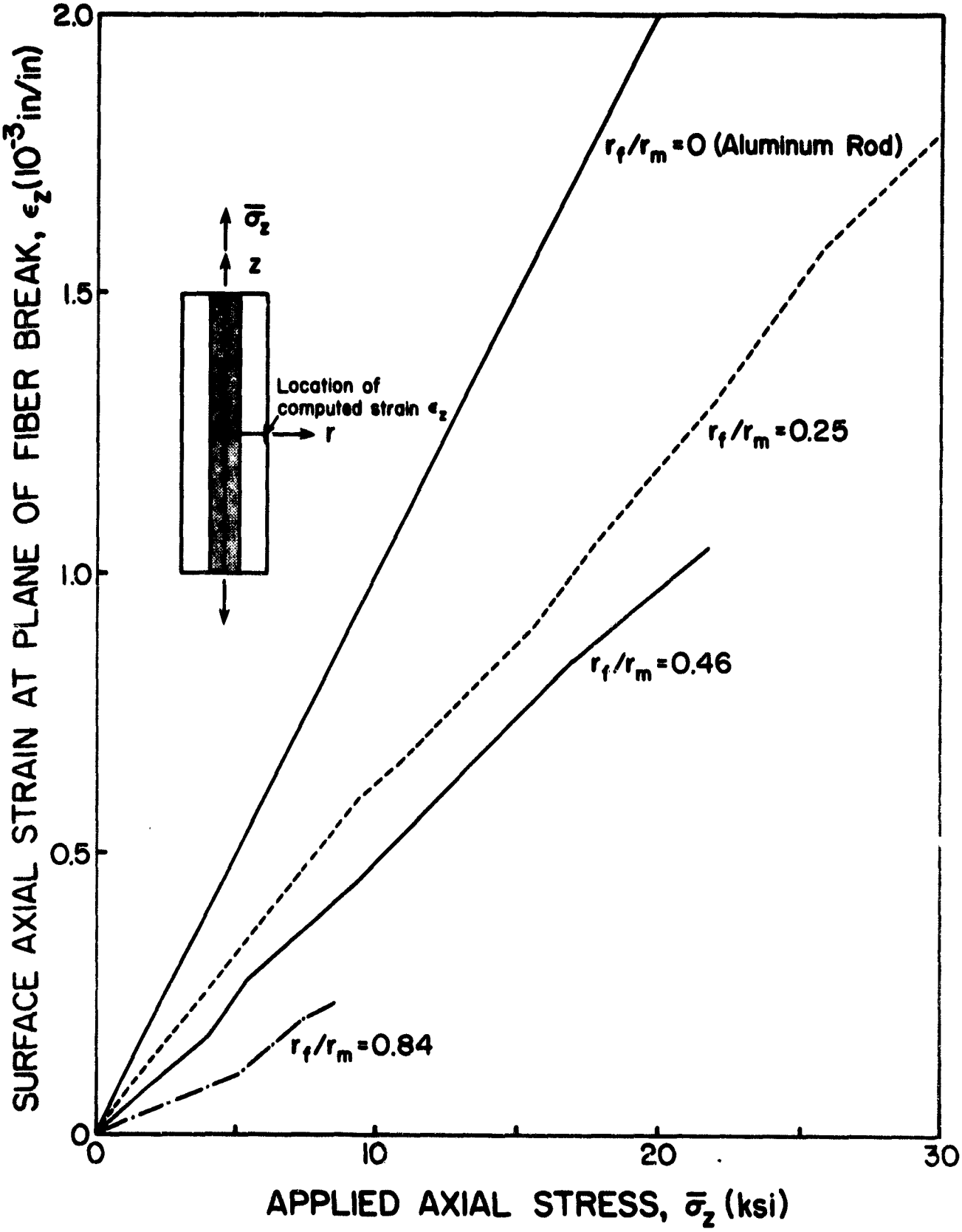

Figure 11. Surface Axial Strain at Plane of Fiber Break Versus Applied Axial Stress

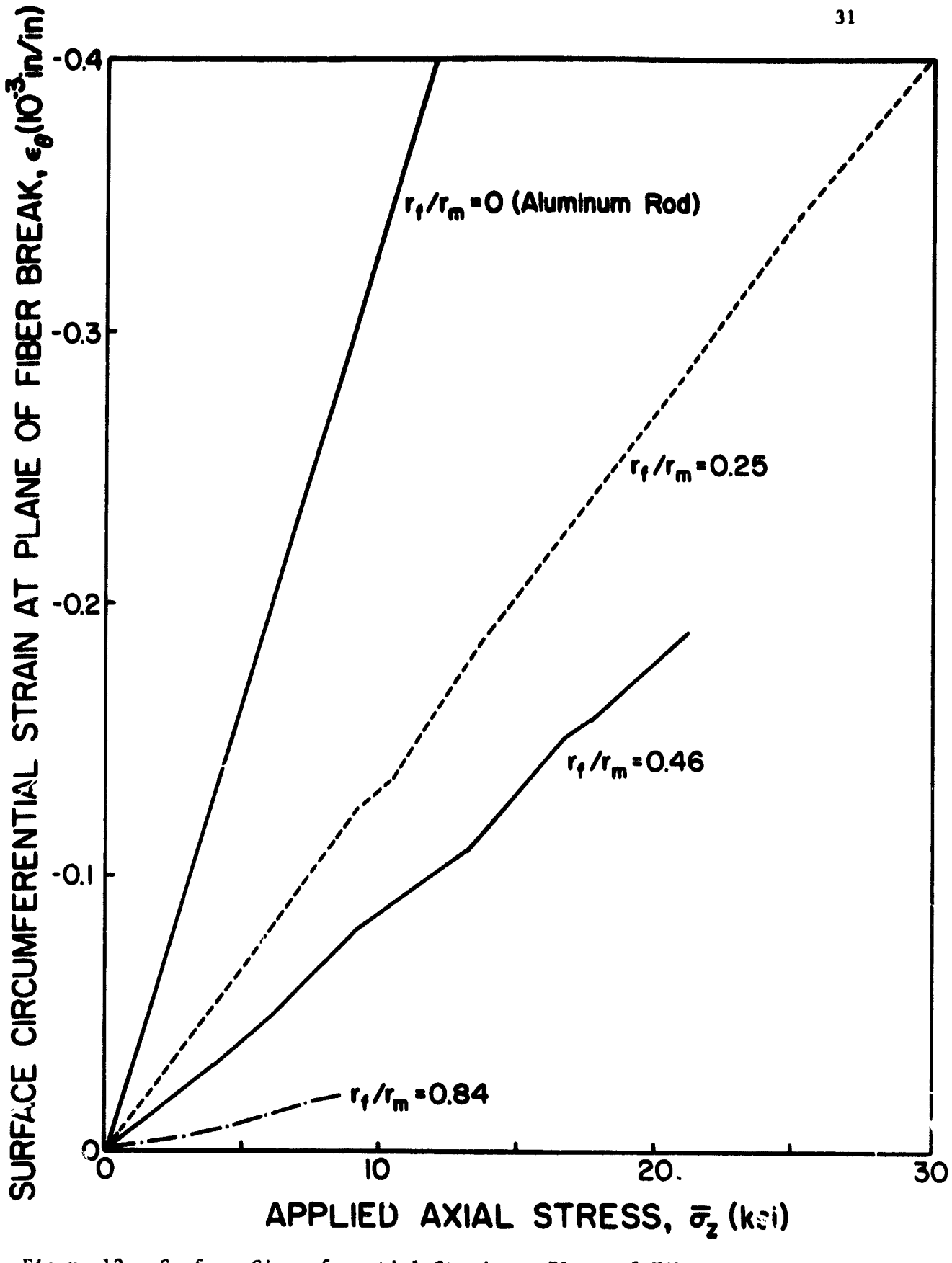

Figure 12. Surface Circumferential Strain at Plane of Fiber Break Versus Applied Axial Stress

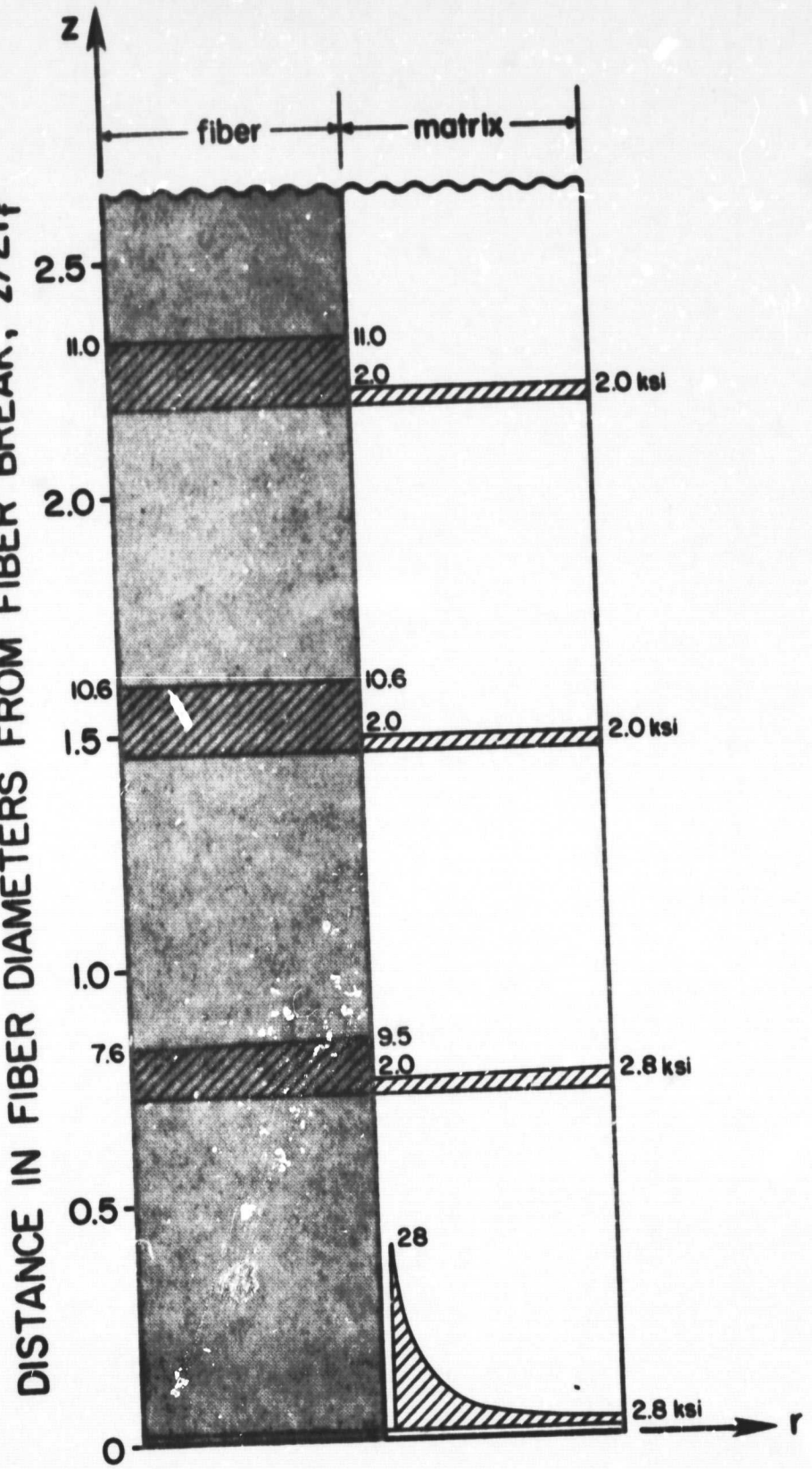

Figure 13. Variation of Axial Normal Stress (in ksi) at Various Sections Along the z-axis ($r_f/r_m = 0.46$)

at increasing distances from the fiber break. The applied axial stress is 4 ksi, well within the elastic range of material response. Right at the plane of the break, the axial normal stress in the fiber is zero, by definition of a free surface. However, the stress concentration in the matrix adjacent to the fiber break is severe, an axial normal stress of 28 ksi being indicated in Figure 13. However, at a distance of about only one and one-half fiber diameters, the stress distribution in both fiber and matrix is almost uniform again.

Figure 14 is a plot of the shear stress along the fiber-matrix interface, plotted as a function of distance in fiber diameters from the fiber break. It is this shear stress which transfers the applied loading across the fiber break, via the matrix sheath. As can be seen, the shear stress builds up very rapidly near the break, but also decays rapidly with increasing distance from the break. At three fiber diameters, the shear stress is negligibly small.

The critical fiber length for complete load transfer, as predicted by the simple mechanics of materials models, is

$$\frac{\ell_c}{d_f} = \frac{1}{2}\frac{\sigma_f}{\tau_m} \tag{5}$$

where σ_f is the fiber axial strength and τ_m is the matrix shear strength; as discussed by Chamis [29]. For the present boron/aluminum composite, σ_f = 500 ksi, τ_m ≈ 26 ksi, d_f = 0.0056 in. Thus, using Eq. (5), ℓ_c/d_f = 9.6, corresponding to a distance of 4.8 fiber diameters from the fiber break in Figures 13 and 14. This is in reasonable agreement with the results obtained in a more rigorous manner in the present study.

The results presented in Figures 13 and 14 do not differ significantly for other r_f/r_m ratios. For example, Figures 15 and 16 are contour plots

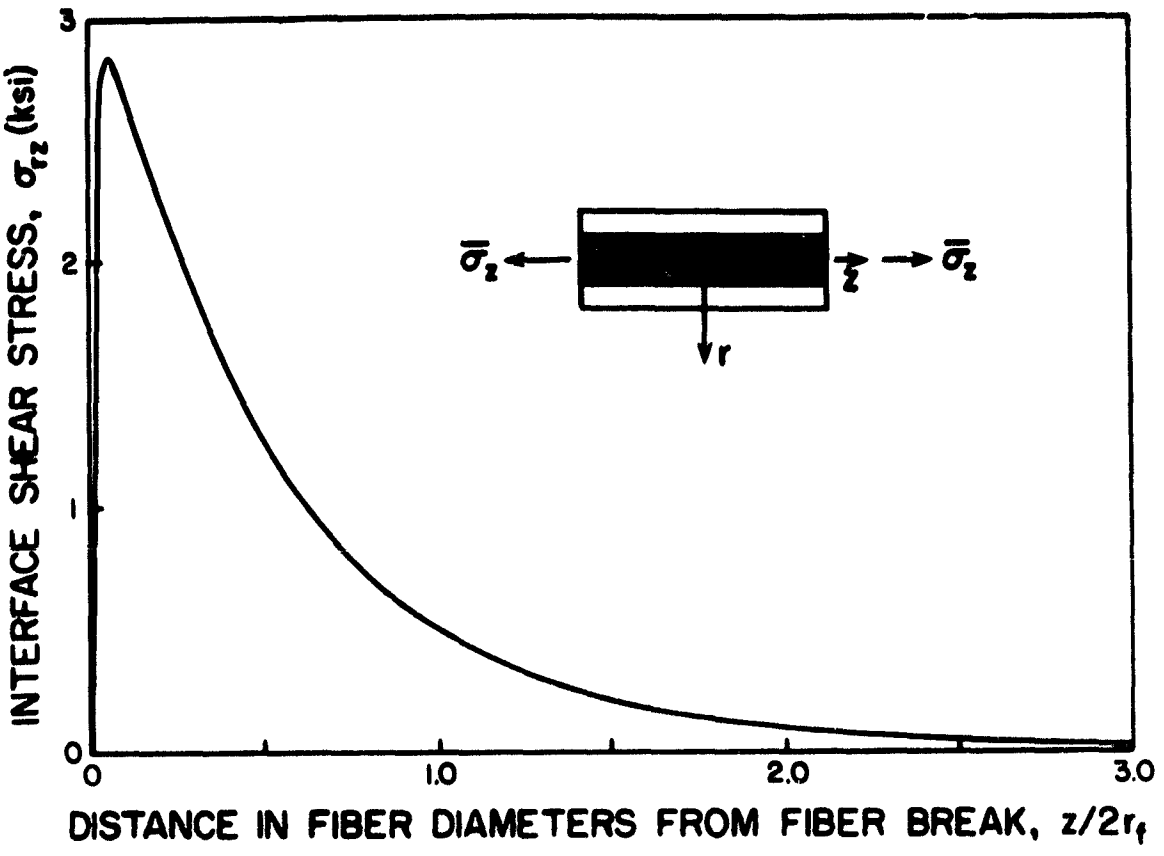

Figure 14. Shear Stress Variation in Aluminum Matrix Along Boron Fiber Interface in the Axial Direction (r_f/r_m = 0.46)

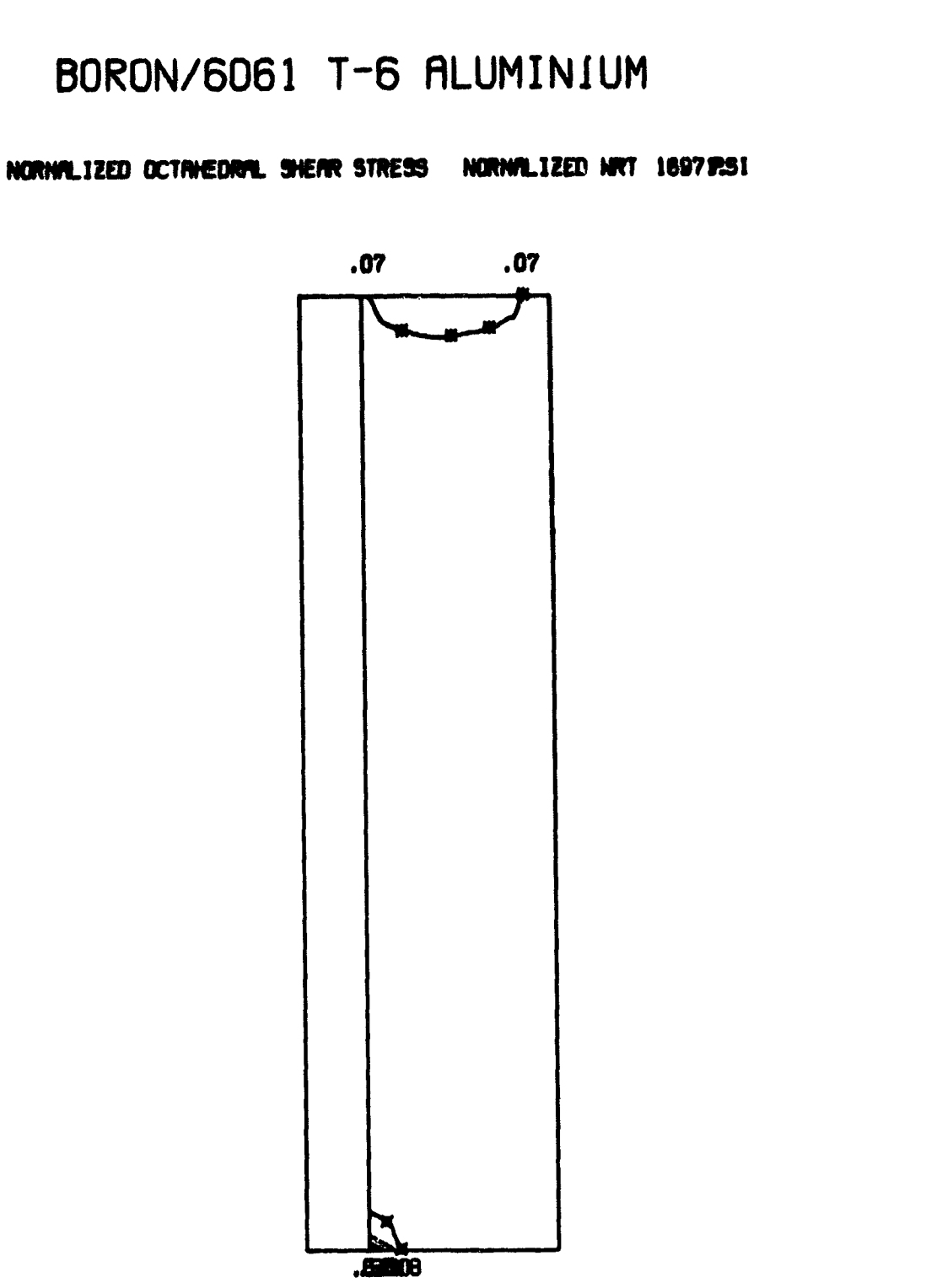

a) Normalized Octahedral Shear Stress

Figure 15. Matrix Stress Contour Plots for r_f/r_m = 0.25

BORON/6061 T-6 ALUMINIUM

MAXIMUM PRINCIPAL STRESS IN KSI

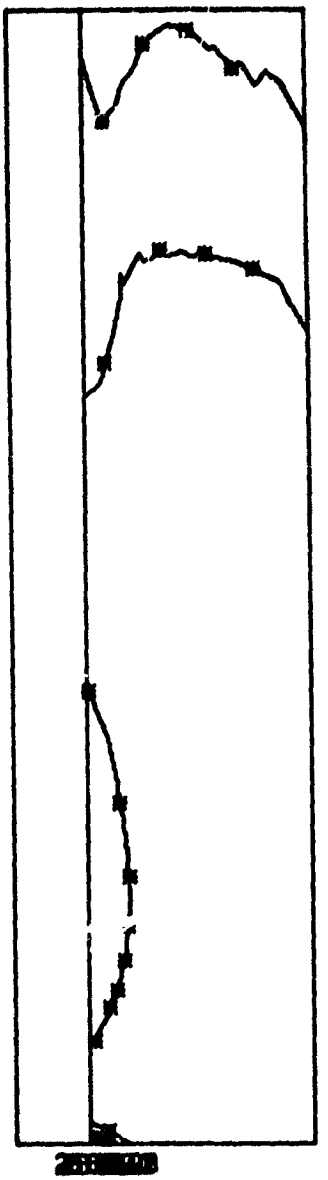

INC 1 TEMPERATURE 0.0 MOISTURE PERCENT 0.0

AVG STRESS R= 0.0 Z= 4000.0

CONTOUR VALUES 3.43 8.28 13.40 18.50 23.60 28.44

b) Maximum Principal Stress

Figure 15 (continued)

BORON/6061 T-6 ALUMINIUM

SHEAR STRESS IN KSI

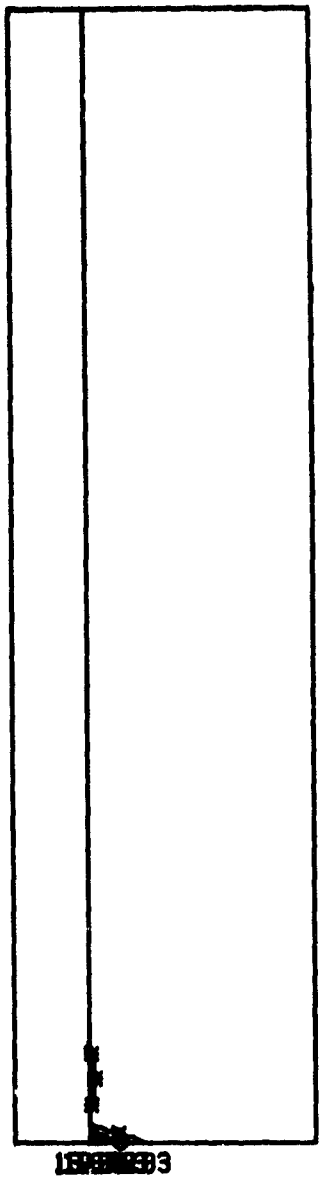

INC 1 TEMPERATURE 0.0 MOISTURE PERCENT 0.0

AVG STRESS R= 0.0 Z= 4000.0

CONTOUR VALUES .99 3.83 6.63 9.82 12.80 15.66

c) Shear Stress

Figure 15 (continued)

BORON/6061 T-6 ALUMINIUM

NORMALIZED OCTAHEDRAL SHEAR STRESS NORMALIZED WRT 16971PSI

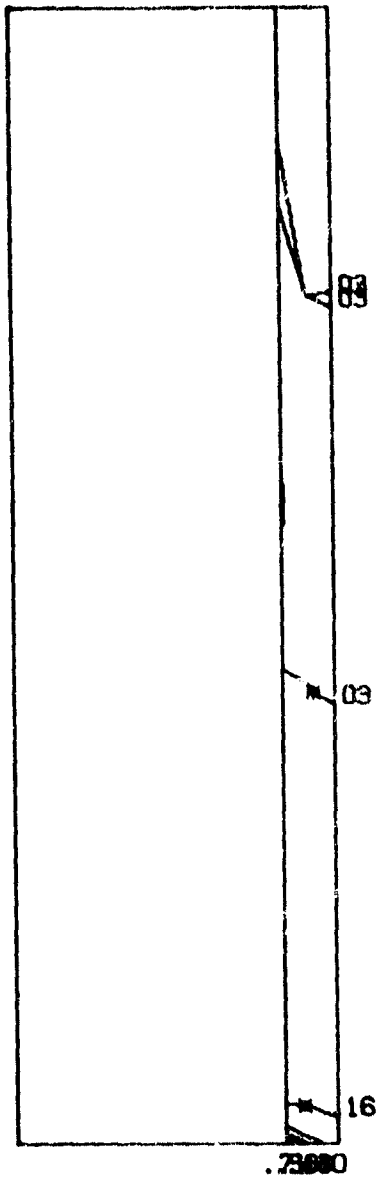

INC 1 TEMPERATURE 0.0 MOISTURE PERCENT 0.0

AVG STRESS R= 0.0 Z= 4000.0

CONTOUR VALUES .03 .16 .30 .44 .58 .71

a) Normalized Octahedral Shear Stress

Figure 16. Matrix Stress Contour Plots for $r_f/r_m = 0.84$

BORON/6061 T-6 ALUMINIUM

MAXIMUM PRINCIPAL STRESS IN KSI

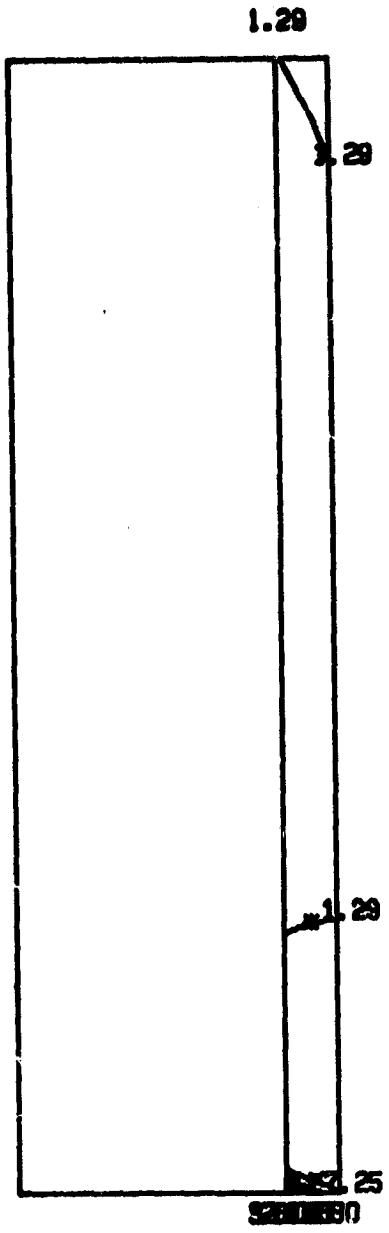

INC 1 TEMPERATURE 0.0 MOISTURE PERCENT 0.0

AVG STRESS R= 0.0 Z= 4000.0

CONTOUR VALUES 1.29 7.25 13.50 19.80 26.10 32.05

b) Maximum Principal Stress

Figure 16 (continued)

BORON/6061 T-6 ALUMINIUM

SHEAR STRESS IN KSI

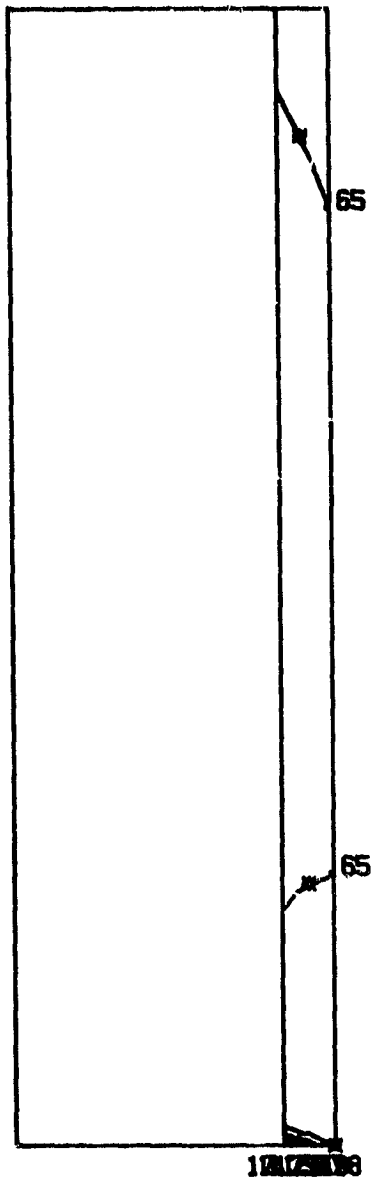

INC 1 TEMPERATURE 0.0 MOISTURE PERCENT 0.0

AVC STRESS R= 0.0 Z= 4000.0

CONTOUR VALUES .65 3.98 7.47 11.00 14.50 17.79

c) Shear Stress

Figure 16 (continued)

of three different stress components throughout the aluminum matrix, for r_f/r_m ratios of 0.25 and 0.84, respectively, for an applied axial stress of 4 ksi. These are computer-generated contour plots; the numerical values of the contours, and the identifying symbols, listed in the legend beneath each plot, are useful in identifying closely spaced contours.

The octahedral shear stress plots of Figures 15a and 16a are significant in that this stress is used to define yield in the present analysis. The contour values have been normalized by dividing by the yield value of the octahedral shear stress, viz, 16.97 ksi, as indicated in the caption. As can be seen in both Figures 15a and 16a, the octahedral shear stresses, although still in the elastic range (the highest normalized values are less than one), are highly localized at the fiber break. It is obvious that first yield will occur at this location.

The maximum principal stress is plotted in Figures 15b and 16b. In the present examples, the maximum normal (i.e., principal) stress failure criterion (see Table 1) was used, as previously noted. The high axial normal stress in the aluminum matrix immediately adjacent to the fiber break (previously indicated in Figure 13 for $r_f/r_m = 0.46$) is obvious, as is the rapid decrease in stress away from this location.

Shear stress contours in the matrix are shown in Figures 15c and 16c. Again, the stress concentration at the fiber break can be readily observed, consistent with the plot for $r_f/r_m = 0.46$ presented in Figure 14.

The stress contour plots of Figures 15 and 16 were for an applied axial stress of only 4 ksi, well within the elastic range of the aluminum matrix material response (see Figure 4). Figure 17 represents a series of normalized octahedral shear stress plots for $r_f/r_m = 0.46$, for increasing levels of applied axial stress, well into the range of inelastic material response and

BORON/ALUMINIUM

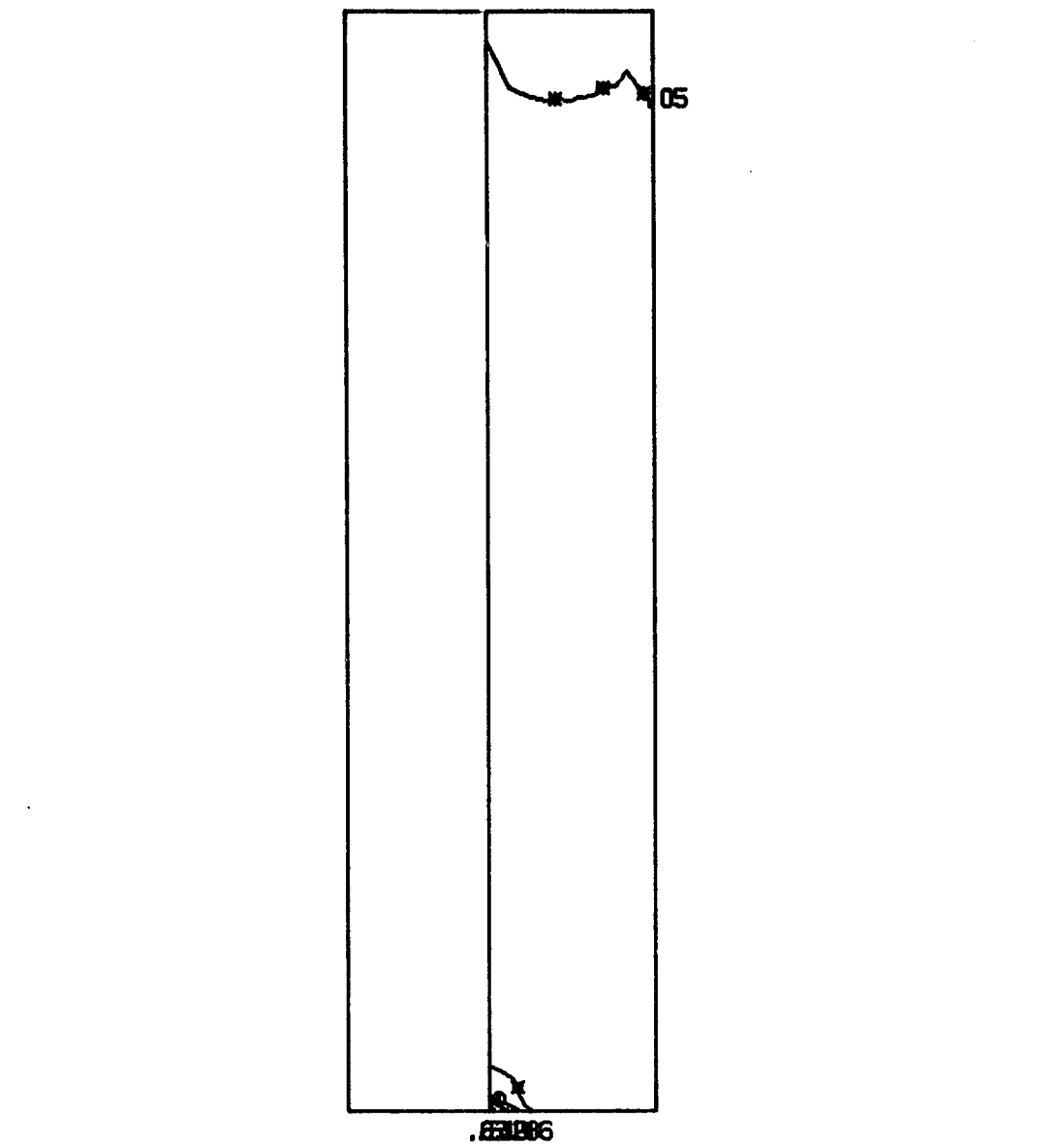

a) Applied Axial Stress $\bar{\sigma}_z$ = 4,000 psi

Figure 17. Matrix Octahedral Shear Stress Contour Plots (Normalized) for r_f/r_m = 0.46, Showing Influence of Crack Propagation

BORON/ALUMINIUM

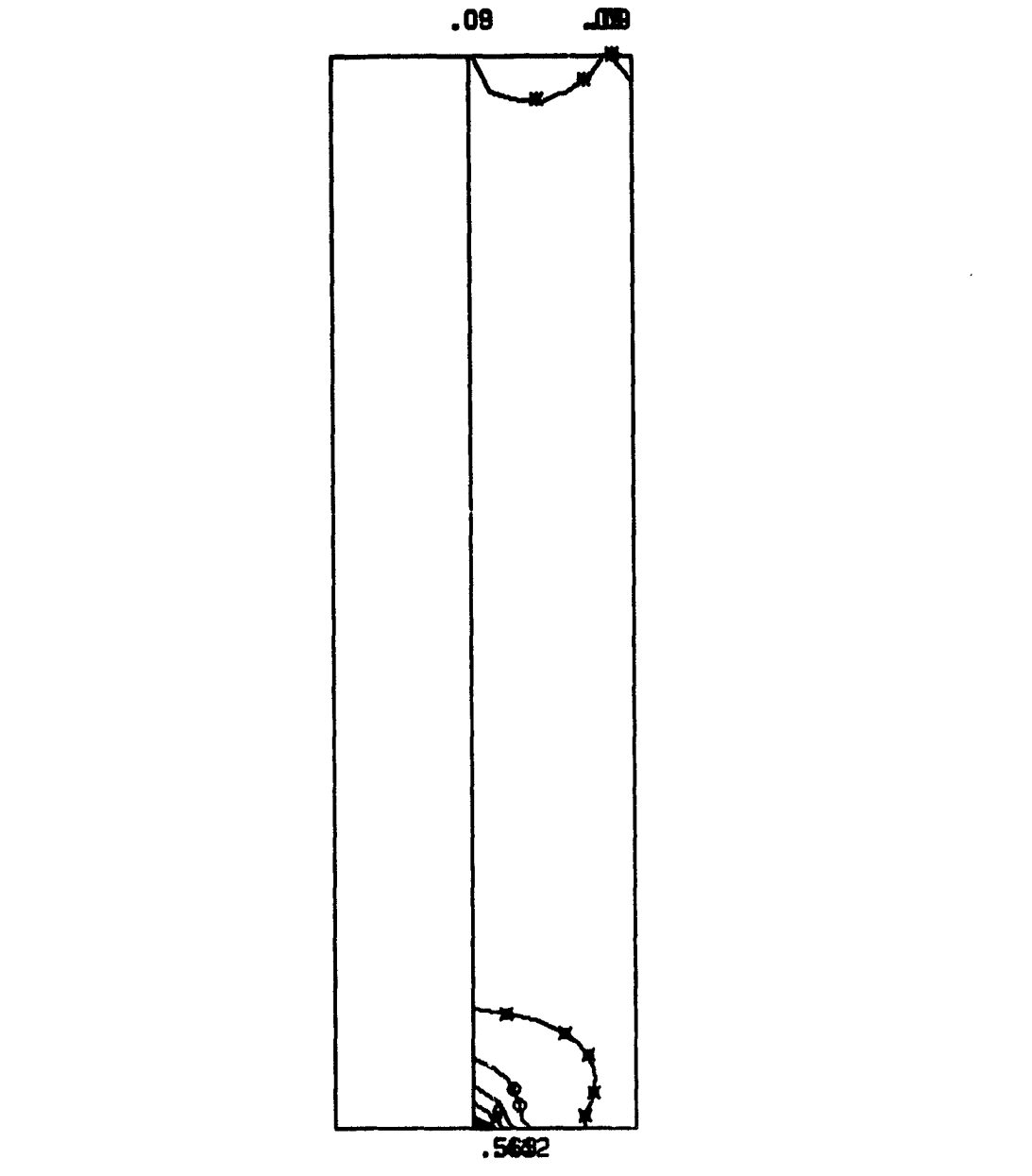

b) Applied Axial Stress $\bar{\sigma}_z$ = 8,915 psi

Figure 17 (continued)

BORON/ALUMINIUM

NORMALIZED OCTAHEDRAL SHEAR STRESS NORMALIZED WRT 16972PSI

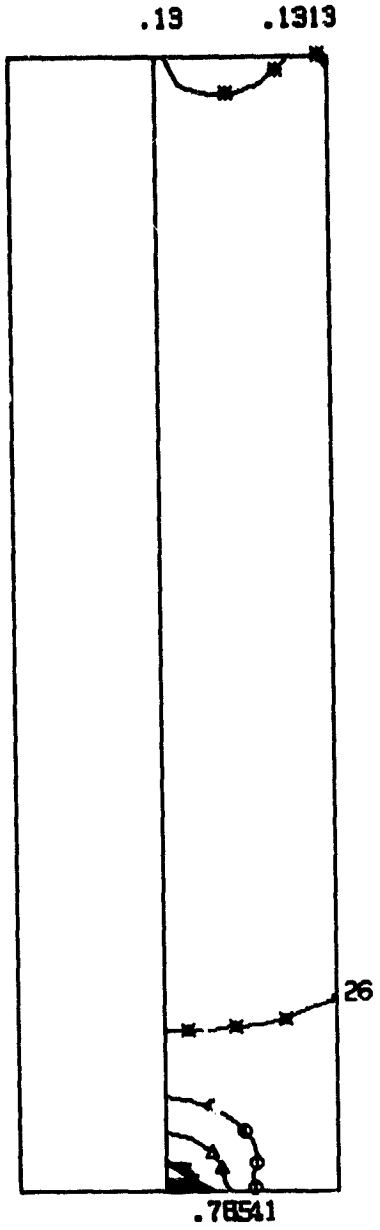

INC 6 TEMPERATURE 0.0 MOISTURE PERCENT 0.0

AVG STRESS R= 0.0 Z= 12,989

CONTOUR VALUES .13 .26 .41 .55 .70 .83

c) Applied Axial Stress $\bar{\sigma}_z$ = 12,989 psi

Figure 17 (continued)

BORON/ALUMINIUM

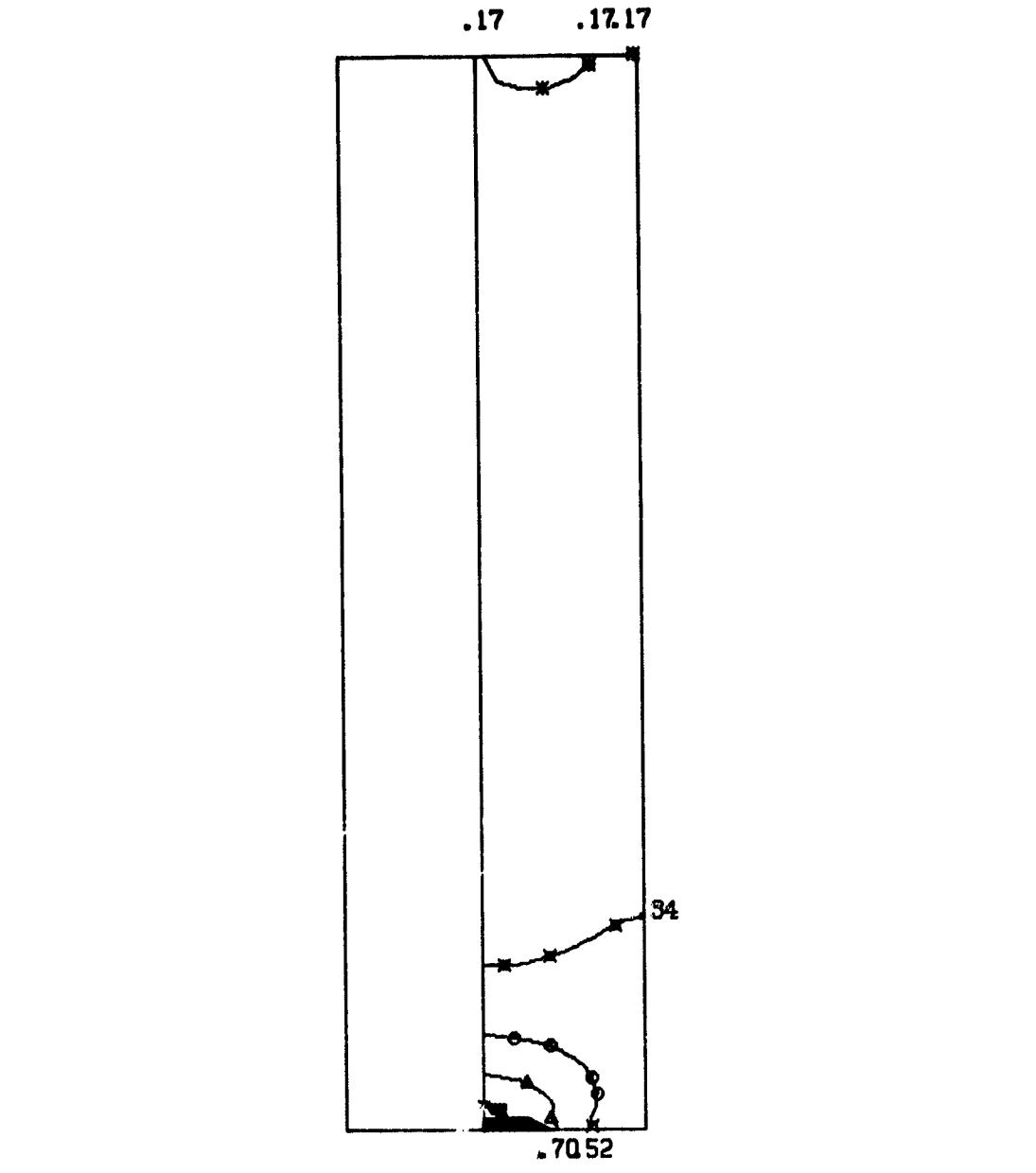

d) Applied Axial Stress $\bar{\sigma}_z$ = 13,696 psi

Figure 17 (continued)

BORON/ALUMINIUM

NORMALIZED OCTAHEDRAL SHEAR STRESS NORMALIZED MRT 1697PSI

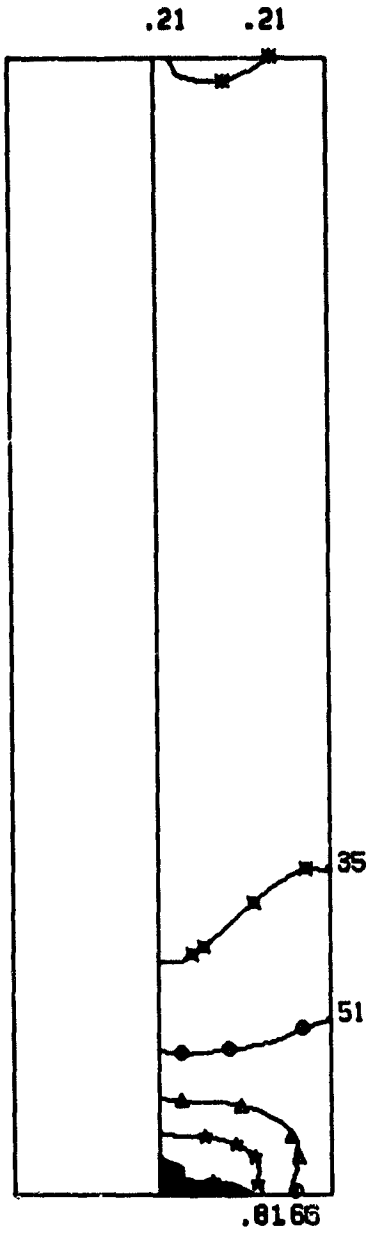

INC 10 TEMPERATURE 0.0 MOISTURE PERCENT 0.0

AVG STRESS R= 0.0 Z= 21,696

CONTOUR VALUES .21 .35 .51 .66 .81 .96

d) Applied Axial Stress $\bar{\sigma}_z$ = 21,696 psi

Figure 17 (continued)

crack propagation. The normalized values of the octahedral shear stress contours are generally less than one only because these plots represent the state of stress immediately following an increment of crack growth (during which the stresses decrease, as indicated in Figure 7).

Beyond the loading state represented by Figure 17d, the applied stress continues to decrease with continued crack propagation (see Figure 7).

It will be noted in Figure 17 that a high stress concentration persists in the region of the propagating crack, as would be expected.

All of the preceeding numerical results were generated using the maximum normal stress failure criterion. The applied axial stress at which the crack initiates, and the ultimate applied stress, are sensitive to the failure criterion utilized. Six different failure criteria have been included in the present analysis, as presented in Table 1 of Section 2.3. Results using each of these theories, for the boron/aluminum composite model with $r_f/r_m = 0.46$, are presented in Table 5.

Much more study will be required to understand the full significance of the different results obtained. It is obvious, however, that the considerable differences exhibited in Table 5 indicate that which failure criterion selected is important, and that it should be relatively straightforward to select the appropriate one, or ones, by correlation with experiment.

In addition to the variation in predicted stress levels, the appropriate failure criterion will also be governed by the correlation between predicted and experimentally observed crack propagation patterns. For example, the maximum normal stress theory and the octahedral shear stress theory, which predict axial tensile ultimate strengths of 21.7 and 24.2 ksi, respectively (Table 5), both indicate a Mode I (opening) failure

Table 5

Influence of Assumed Failure Theory on Crack Propagation in a Boron/Aluminum Composite, $r_f/r_m = 0.46$

Failure Theory	Crack Initiation Stress (psi)	Ultimate Strength (psi)
1. Maximum Normal Stress	5,666	21 [illegible]96
2. Maximum Shear Stress	4,848	36,038
3. Octahedral Shear Stress	7,923	24,196
4. Tsai-Hill	4,693	40,356
5. Hoffman	2,262	14,750
6. Tsai-Wu (Modified)	2,497	14,225

mode. The maximum normal stress theory results were presented in Figure 8. The octahedral shear stress theory results are shown in Figure 18. Mode II (shear) failure is predominate when the maximum shear stress or Tsai-Hill failure criterion is assumed, the predicted ultimate strengths being 36.0 and 40.4 ksi, respectively. The Hoffman and Tsai-Wu failure criteria, both of which exhibit predominently Model I type failures, predicted ultimate strengths of 14.8 and 14.2 ksi, respectively. Figure 19 represents the crack propagation pattern predicted using the maximum shear stress failure criterion. As can be seen, there is a strong tendency for the crack to propagate along the fiber-matrix interface, due to the high shear stress in this region (as shown in Figure 14). Of course, for complete failure (fracture) of the model composite to occur due to the applied axial tensile stress, the matrix crack must eventually propagate to the outer radius, as shown in the last sketch of Figure 19.

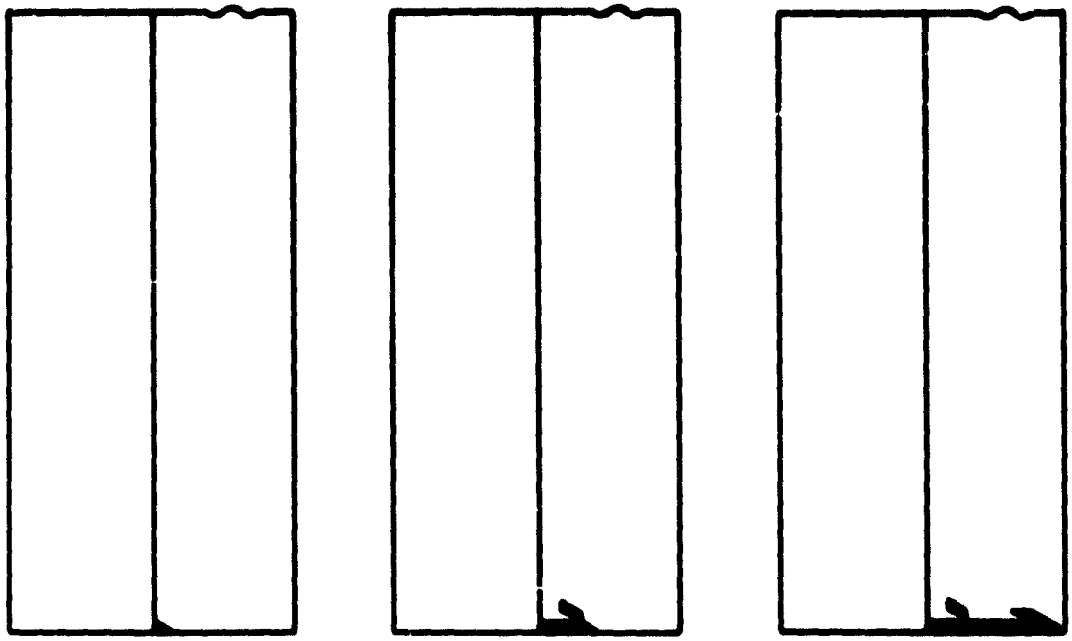

Figure 18. Crack Propagation in a Boron/Aluminum Composite Model as Predicted by the Octahedral Shear Stress Theory, r_f/r_m=0.46 (stresses in psi)

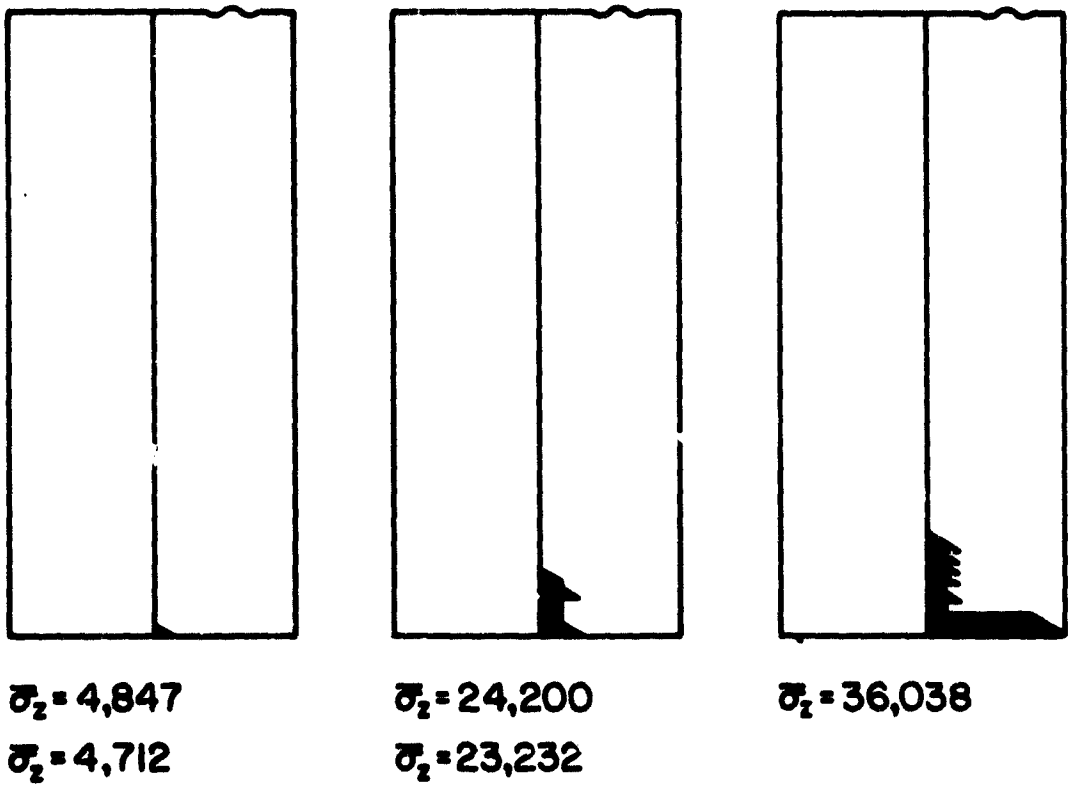

Figure 19. Crack Propagation in a Boron/Aluminum Composite Model as Predicted by the Maximum Shear Stress Theory, r_f/r_m = 0.46 (stresses in psi)

4.3 Energy of Crack Propagation in a Model Composite

An estimation of the absorption of energy associated with crack propagation is an important aspect of any fracture mechanics study. A significant amount of information can be obtained by studying the variation of energy levels during crack propagation

4.3.1 Evaluation of Fracture Energy

The total potential energy, V , of a cracked body consists of elastic strain energy, U_e, the energy absorbed in the plastic region, U_p, surface energy, U_s, and the potential energy of external loads, Ω. A balance of these energies during crack propagation, as presented by Griffith, Irwin, and Orowan [30] forms the basis of linear elastic fracture mechanics (LEFM).

The above criterion states that a crack propagates when the energy release rate, G, is equal to the energy absorbed, R, i.e., G=R.

Since the energy release rate and the stress intensity factor, K, are related when $G=G_c$ (critical value of G), the corresponding stress intensity factor is K_c. This critical K value is the so-called fracture toughness (i.e., resistance to crack growth). A significant amount of work has been done to characterize the fracture toughness as a material property. It has been observed that the crack resisting parameter R is not a constant, but increases as the crack extends due to the increase in the plastic enclave absorbing more and more energy. The fact that R is not a constant, but increases as the crack extends, explains the observed stable crack growth. Plots of G and R as functions of crack length a (see Figure 5), for a range of initial crack lengths, are known as R-curves. The R-curves are very useful in understanding the behaviour of crack propagation.

4.3.2 Calculation of Total Potential Energy and Energy Release Rate

In the present finite element analysis, the total potential energy is calculated at each load increment. The total potential energy, V, is given as

$$V = U + \Omega \tag{6}$$

where U is the total strain energy (U_e plus U_p) and Ω is the potential energy of the external loads. Surface energy is assumed negligible.

The total strain energy U is given by

$$U = \sum_{i=1}^{n} \int_{V_i} U_{o_i} \, dV_i \tag{7}$$

where U_{o_i} = strain energy density in a finite element

$= \frac{1}{2}\{\sigma\}^T\{d\epsilon\}$

n = number of finite elements

V_i = volume of an element

The potential energy of the external loads is

$$\Omega = -\sum P_j \delta_j \tag{8}$$

where δ_j is the displacement of the loaded boundary point j.

The energy release rate, G, is then calculated as

$$G = \frac{V_1 - V_2}{\Delta a} \tag{9}$$

where V_1 is the total potential energy at the initiation of the crack and V_2 is the total potential energy after the crack has extended an increment Δa.

Figure 20 shows the variations of total potential energy in the boron/aluminum, broken-fiber model (Figure 1) as the crack extends.

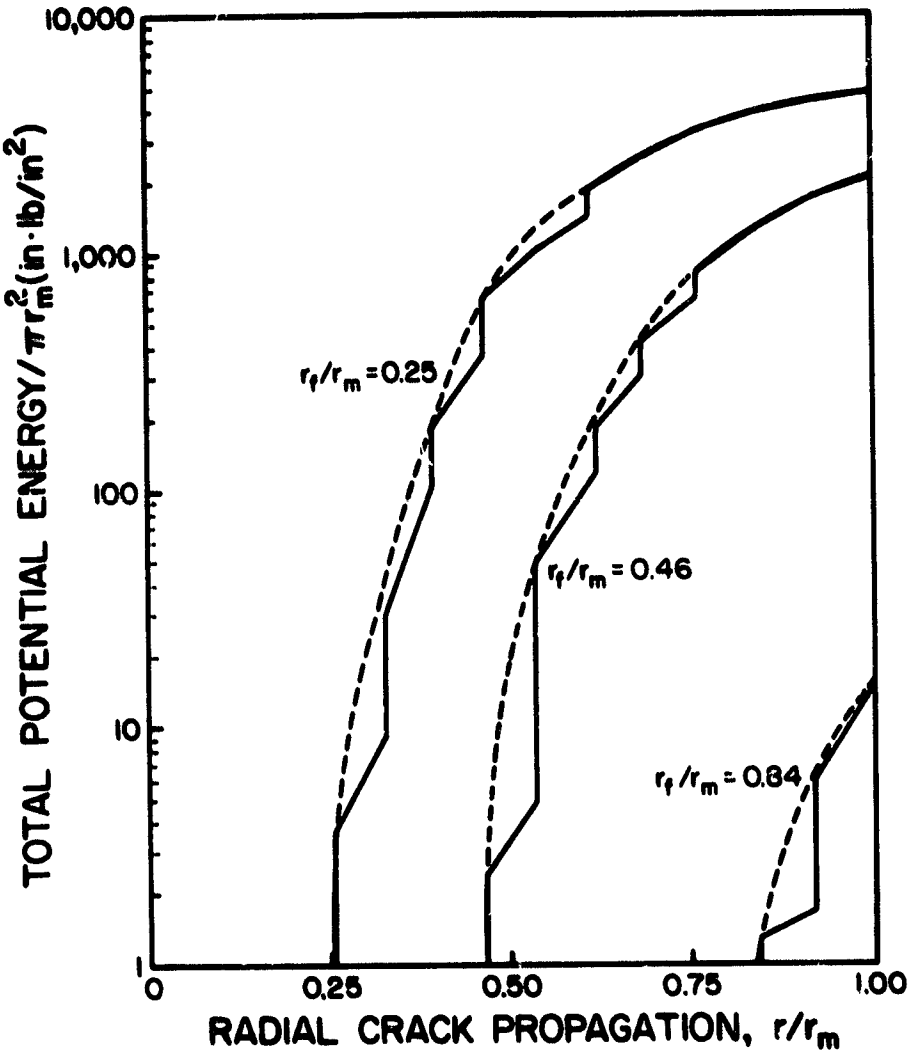

Figure 20. Total Potential Energy (Normalized) Versus Crack Extension

Since, in the present finite element analysis, cracks extend in finite lengths (equal to the size of the failed element), a step variation is observed. The dashed lines indicate the smoothed curves.

In Figure 21, R-curves corresponding to three different initial crack lengths (equal to the broken fiber radius) are plotted. It can be observed that the energy release (i.e., the energy absorbed) is higher for the smaller initial crack length, and attains an unstable condition earlier than for the larger initial crack length geometries.

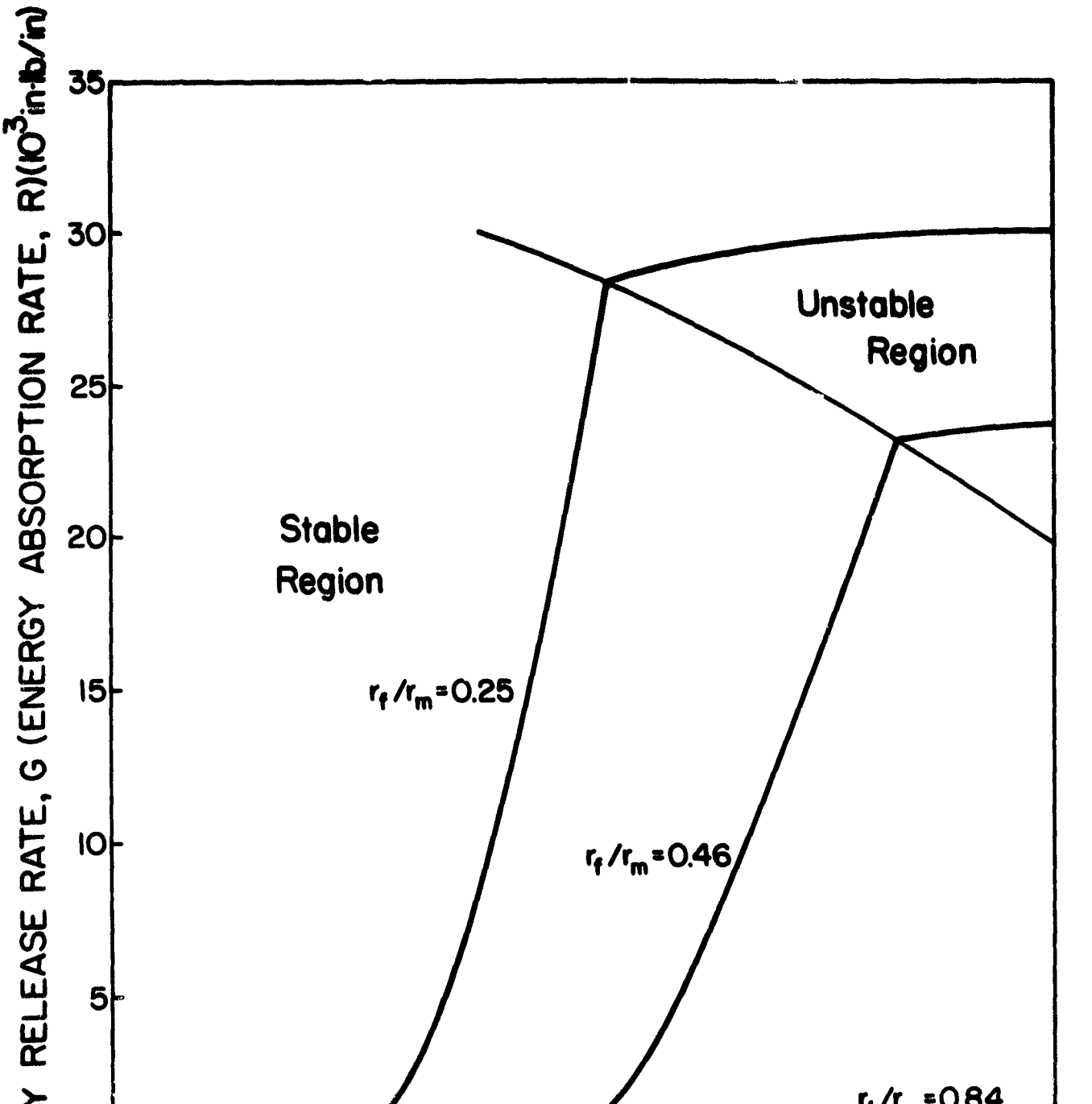

Figure 21. Energy Absorption During Crack Propagation in a Boron/Aluminum Axisymmetric Model Composite

SECTION 5

DISCUSSION

The primary purpose in developing the axisymmetric analysis, with inelastic crack propagation capability, was to permit the correlation of analytical predictions of crack propagation and failure with experimental measurements. It is the experimental work which encourages the use of a simple composite model. By using a simple test specimen, experimental measurements are relatively easy to perform, and interpret.

At the present time, experimental data for the boron/aluminum composite, single broken fiber model is not yet available. The original plan was that NASA-Lewis would generate this data. It now appears that this may not be possible. One alternative is to undertake this as a subsequent study at the University of Wyoming.

Another alternative is to model an epoxy-matrix composite, and then correlate the predicted response with available single fiber composite data. For example, preliminary discussions with Drzal [31] indicate that he may have suitable data for a graphite/epoxy model composite. To establish that the present analysis will perform as well in predicting stable crack propagation in an epoxy matrix, a much less ductile material than the aluminum matrix used in obtaining the present results, another series of computer runs were made, for both glass/epoxy and graphite/epoxy. These results are summarized in Reference [32]. In general, the results obtained were similar to those presented here, in the sense of stable cracks being propagated. One obvious and distinct advantage of using a polymer matrix is its transparency. The propagating crack can be observed directly, and measurements of such parameters as crack opening displacement (the gap

width between the ends of the broken fiber) can be made optically. For the metal matrix composite model, an X-ray technique or something similar will be required.

References

1. Murphy, D.P., and Adams, D.F., "Energy Absorption Mechanisms During Crack Propagation in Metal Matrix Composites," Report UWME-DR-901-103-1, Department of Mechanical Engineering, University of Wyoming, Laramie, Wyoming, October 1979.

2. Miller, A.K., and Adams, D.F., "Micromechanical Aspects of the Environmental Behavior of Composite Materials," Report UWME-DR-701-111-1, Department of Mechanical Engineering, University of Wyoming, Laramie Wyoming, January 1977.

3. Adams, D.F., and Miller, A.K., "Hygrothermal Microstresses in a Unidirectional Composite Exhibiting Inelastic Material Behavior," Journal of Composite Materials, Vol. 11, No. 3, July 1977, pp. 285-299.

4. Miller, A.K., and Adams, D.F., "Inelastic Finite Element Analysis of a Heterogeneous Medium Exhibiting Temperature and Moisture Dependent Material Properties," Fibre Science and Technology, Vol. 13, No. 2, March-April 1980, pp. 135-153.

5. Adams, D.F., "High Performance Composite Materials for Vehicle Construction; An Elastoplastic Analysis of Crack Propagation in a Unidirectional Composite," Report R-1070-PR, The Rand Corporation, Santa Monica, California, March 1973.

6. Repnau, T. and Adams, D.F., "A Finite Element Computer Program for Elastoplastic Analysis of Crack Propagation in a Unidirectional Composite," Report R-1392-PR, The Rand Corporation, Santa Monica, California, October 1973.

7. Adams, D.F., "Elastoplastic Crack Propagation in a Transversely Loaded Unidirectional Composite," Journal of Composite Materials, Vol. 8, No. 1, January 1974, pp. 38-54.

8. Adams, D.F., "A Micromechanical Analysis of Crack Propagation in an Elastoplastic Composite Material," Fibre Science and Technology, Vol. 7, No. 4, October 1974, pp. 237-256.

9. Adams, D.F., and Murphy, D.P., "Analysis of Crack Propagation as an Energy Absorption Mechanism in Metal Matrix Composites," Report UWME-DR-101-102-1, Department of Mechanical Engineering, University of Wyoming, Laramie, Wyoming, February 1981.

10. Segerlind, L.J., Applied Finite Element Analysis, John Wiley & Sons, Inc., New York, NY (1976).

11. Branca, T.R., "Creep of a Unidirectional Metal Matrix Composite Subjected to Axial and Normal Lateral Loads," TAM Report 341, Department of Theoretical and Applied Mechanics, University of Illinois, Urbana, Illinois, June 1971.

12. Jones, R.M., Mechanics of Composite Materials, McGraw-Hill Book Company, New York, NY (1975).

13. Boresi, A.P., Sidebottom, O.M., Seely, F.B., and Smith, J.O., Advanced Mechanics of Materials, Third Edition, John Wiley & Sons, Inc., New York, NY (1978).

14. Chamis, C.C., "Failure Criteria for Filamentary Composites," Composite Materials: Testing and Design, ASTM STP 460, American Society for Testing and Materials, Philadelphia, Pennsylvania, 1969, pp. 336-351

15. Sendeckyj, G.P., "A Brief Survey of Empirical Multiaxial Strength Criteria for Composites," Composite Materials: Testing and Design (Second Conference), ASTM STP 497, American Society for Testing and Materials, Philadelphia, Pennsylvania, 1972, pp. 41-51.

16. Kaminski, B.E. and Lantz, R.B., "Strength Theories of Failure for Anisotropic Materials", Composite Materials: Testing and Design, ASTM STP 460, American Society for Testing and Materials, Philadelphia, Pennsylvania, 1969, pp. 160-169.

17. Hoffman, O., "The Brittle Strength of Orthotropic Materials," Journal of Composite Materials, Vol. 1, No. 2, April 1967, pp. 200-206.

18. Tsai, S.W., and Wu, E.M., "A General Theory of Strength for Anisotropic Materials," Journal of Composite Materials, Vol. 5, No. 1, Jan. 1971, pp. 58-80.

19. Wu, E.M., "Optimal Experimental Measurements of Anisotropic Failure Tensors," Journal of Composite Materials, Vol. 6, No. 4, October 1972, pp. 472-489.

20. Narayanaswami, R. and Adelman, H.M., "Evaluation of the Tensor Polynomial and Hoffman Strength Theories for Composite Materials," Journal of Composite Materials, Vol. 11, No. 4, October 1977, pp. 366-377.

21. Richard, R.M., and Blacklock, J.R., "Finite Element Analysis of Inelastic Structures," AIAA Journal, Vol. 7, No. 3, March 1969, pp. 432-438.

22. Military Handbook 5A, "Metallic Materials and Elements for Aerospace Vehicle Structures," Department of Defense, Washington, D.C., 1966.

23. DiCarlo, J.A., "Mechanical and Physical Properties of Modern Boron Fibers," NASA Technical Memorandum NASA TM-73882, NASA-Lewis Research Center, Cleveland, Ohio, April 1978.

24. Hilton, P.D., and Sih, G.C., "Applications of Finite Element Method to the Calculations of Stress Intensity Factors", Mechanics of Fracture, Vol. 1, Ed. G. C. Sih, Noordhoff Int. Pub., Leyden (1973).

25. Williams, M.L., "On the Stress Distribution at the Base of a Stationary Crack", Journal of Applied Mechanics, Vol. 24, No. 1, March 1957, pp. 109-114.

26. Tada, H., Paris, P.C., and Irwin, G.R., The Stress Analysis of Cracks Handbook, Del Research Corporation, St. Louis, Missouri (1978).

27. Rooke, D.P. and Cartwright, D.J., Compendium of Stress Intensity Factors, Her Majesty's Stationery Office, London, England (1976).

28. Paris, P.C. and Sih, G.C., Fracture Toughness Testing and its Applications, ASTM STP 381, American Society for Testing and Materials, Philadelphia, Pennsylvania, 1965, pp. 426-483.

29. Chamis, C.C., "Mechanics of Load Transfer at the Fiber/Matrix Interface," NASA Technical Note NASA TN D-6588, NASA-Lewis Research Center, Cleveland, Ohio, February 1972.

30. Tetelman, A.S., and McEvilly, Jr., A.J., Fracture of Structural Materials , John Wiley & Sons, Inc., New York, NY (1967).

31. Private Conversation with L.T. Drzal, Air Force Materials Laboratory, Dayton, Ohio, June, 1981.

32. Adams, D.F., "Micromechanical Failure Predictions for Polymer-Matrix Composites," Proceedings of the Fifth Churchill Conference on Deformation, Yield and Fracture of Polymers, University of Cambridge, Cambridge, England, March 1982.